Contrib Mineral Petrol (1992) 110:68–86

Contributions to Mineralogy and Petrology

Geochemical evolution of Jurassic diorites from the Bristol Lake region, California, USA, and the role of assimilation

Edward D. Young[1]*, Joseph L. Wooden[2], Yuch-Ning Shieh[3], and Daniel Farber[1]

[1] Department of Geological Sciences, University of Southern California, Los Angeles, CA 90089, USA
[2] U.S. Geological Survey, 345 Middlefield Rd., Menlo Park, CA 94025, USA
[3] Department of Earth and Atmospheric Sciences, Purdue University, West Lafayette, IN 47907, USA

Received January 2, 1991 / Accepted June 14, 1991

Abstract. Late Jurassic dioritic plutons from the Bristol Lake region of the eastern Mojave Desert share several geochemical attributes with high-alumina basalts, continental hawaiite basalts, and high-K arc andesites including: high K_2O concentrations; high Al_2O_3 (16–19 weight %); elevated Zr/TiO_2; LREE (light-rare-earth-element) enrichment (La/Yb_{CN} = 6.3–13.3); and high Nb. Pearce element ratio analysis supported by petrographic relations demonstrates that P, Hf, and Zr were conserved during differentiation. Abundances of conserved elements suggest that dioritic plutons from neighboring ranges were derived from similar parental melts. In the most voluminous suite, correlated variations in elemental concentrations and $(^{87}Sr/^{86}Sr)_i$ indicate differentiation by fractional crystallization of hornblende and plagioclase combined with assimilation of a component characterized by abundant radiogenic Sr. Levenberg-Marquardt and Monte Carlo techniques were used to obtain optimal solutions to non-linear inverse models for fractional crystallization-assimilation processes. Results show that the assimilated material was chemically analogous to lower crustal mafic granulites and that the mass ratio of contaminant to parental magma was on the order of 0.1. Lack of enrichment in ^{18}O with differentiation is consistent with the model results. Elemental concentrations and O, Sr, and Nd isotopic data point to a hydrous REE-enriched subcontinental lithospheric source similar to that which produced some Cenozoic continental hawaiites from the southern Cordillera. Isotopic compositions of associated granitoids suggest that partial melting of this subcontinental lithosphere may have been an important process in the development of the Late Jurassic plutonic arc of the eastern Mojave Desert.

Introduction

Petrogenetic studies of Mesozoic plutons have revealed a wealth of information about the geochemical development of crust and underlying mantle in the Mojave Desert region (e.g. Miller et al. 1990). The majority of studies have focused on plutons of Cretaceous age (cf. Fox and Miller 1990). Comparatively few petrogenetic studies have been conducted on the older Jurassic intrusives in the region. The dearth of Jurassic studies exists in part because plutonic rocks of this age typically are affected by sodium metasomatism and consequently yield limited petrogenetic information (Fox and Miller 1990).

In this paper we present results of an analysis of the geochemical evolution of a Late Jurassic dioritic pluton from the Bristol Lake region of the Mojave Desert (Fig. 1). The primitive composition of this mafic pluton relative to surrounding granitoids and the paucity of metasomatism permit identification of differentiation processes and possible source rocks. Similarities in elemental and isotopic compositions suggest that the neighboring more altered Late Jurassic diorites of the region may have originated by the same processes elucidated by this study of the unaltered pluton.

Results show that the Bristol Lake diorite parental melts were derived from a hydrous LREE-enriched subcontinental lithosphere and evolved by combined fractional crystallization and assimilation of mafic lower crust. Comparison with Sr and Nd isotopic compositions of other Jurassic plutons from the eastern Mojave Desert region suggests that interaction between continental crust and subcontinental lithosphere may have been an important process during this time period. Magma generation in the subcontinental lithosphere is consistent with suggestions that the eastern Mojave Desert was part of a zone of protracted extensional tectonic activity during the Jurassic.

Analytical methods

Whole-rock elemental concentrations

Whole-rock analyses were performed on an automated wavelength dispersive X-ray fluorescence spectrometer at the University of

* *Present address*: Geophysical Laboratory, Carnegie Institution of Washington, 5251 Broad Branch Road NW, Washington D.C. 20015-1305
Offprint requests to: E. D. Young

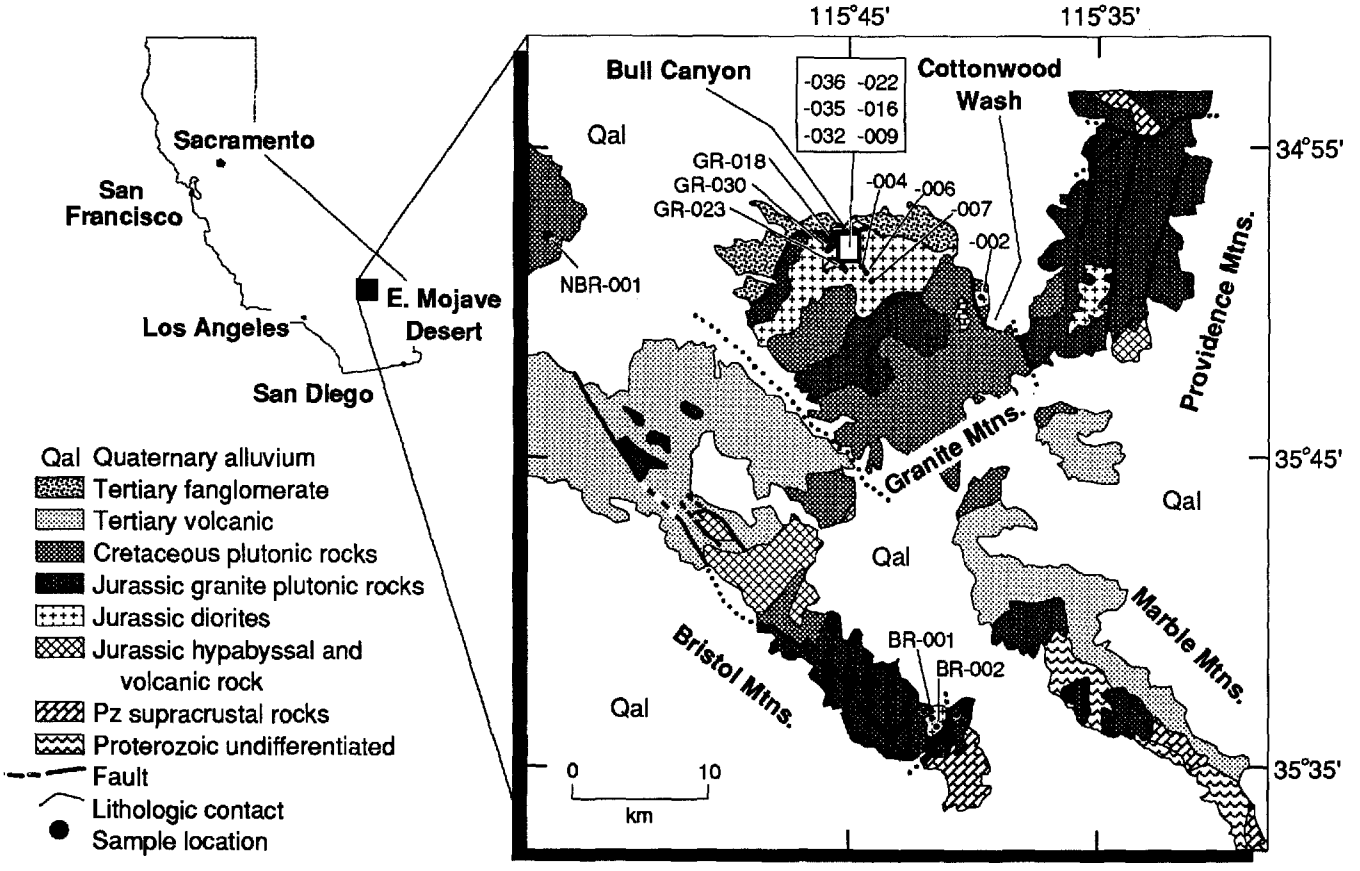

Fig. 1. Generalized geologic map of the Bristol Lake region based on mapping by Howard et al. (1989) and Fox and Miller (1990). Sample localities for this study are also shown

Southern California. Volatile loss on ignition was determined from weight loss of oven-dried powders (110°C) following heating in a muffle furnace at 1000°C. Major elements were analyzed using 30 mm diameter fused discs prepared with a $Li_2 \cdot O \cdot 2B_2O_3 - Li_2CO_3 - La_2O_3$ flux following the methods described by Norrish and Hutton (1969) and Harvey et al. (1973). Mass-absorption corrections were applied iteratively using the coefficients of Heinrich (1964). Trace-element analyses were performed on 30 mm briquettes of sample-cellulose mixtures using Rh-target Compton scattered peaks for matrix corrections. The majority of samples were ground to 200 mesh in agate. Samples ground in tungsten carbide showed significant Ta contamination but no detectable Nb contamination. Precision of major-element determinations is 1% (1σ) or better. Precision of trace-element analyses varies from 1% for Rb and Sr to 15% for Hf.

Oxygen isotopes

Oxygen was extracted from ~ 15 mg splits of whole-rock powders and mineral separates with BrF_5 in sealed Ni reaction vessels at 560°C using a modification of the technique described by Clayton and Mayeda (1963). Samples were loaded in a dry box. Low-temperature pre-fluorination was used to remove adsorbed H_2O. Liberated O_2 was converted to CO_2 by reaction with a resistance-heated graphite rod in the presence of platinum.

Isotope ratios were measured on a Nuclide 3-60 RMS dual-collector gas-ratio mass spectrometer at Purdue University. Values are reported in standard per mil deviations (δ) from V-SMOW (Vienna Standard Mean Ocean Water). Replicate analyses of the NBS-28 quartz standard during this study yielded a mean $\delta^{18}O_{V-SMOW}$ of 9.7 ± 0.2 per mil and manometrically measured yields of 98 to 100%.

Strontium and Nd isotopes

Whole-rock Sr and Nd isotope determinations were made using 100 mg splits of sample powder dissolved with standard HF, HNO_3, and HCl dissolution techniques. A mixed ^{149}Sm-^{150}Nd spike was added for isotope-dilution determination of Sm and Nd concentrations. Rb and Sr concentrations were obtained with X-ray fluorescence spectrometry. Sr and rare-earth elements were separated on ion-exchange columns using standard methods.

Sr and Nd isotopic abundances and concentrations of Sm and Nd were measured on the Finnigan MAT 261 single-collector and Finnigan MAT 262 multiple-collector solid-source mass spectrometers housed at the U.S. Geological Survey, Branch of Isotope Geology in Menlo Park. Measured isotopic ratios are precise to 0.1% or better. Isotopic data for Sr are normalized to $^{86}Sr/^{88}Sr = 0.1194$. Isotopic data for Nd are normalized to $^{146}Nd/^{144}Nd = 0.7219$. Replicate analyses of NBS-987 yielded an average measured $^{87}Sr/^{86}Sr$ of 0.71027 with an external precision of ± 0.00002. Replicate analyses of USGS BCR-1 gave an average measured $^{143}Nd/^{144}Nd$ of 0.512633 with an external precision of ± 0.000010.

Uranium-lead geochronology

Zircon dissolutions and U-Pb separations were performed using a modification of the method described by Krogh (1973). Aliquotes of dissolved sample were spiked with a mixed ^{235}U-^{208}Pb tracer for isotope dilution determinations of U and Pb concentrations.

Isotope ratios were measured on the MAT 261 mass spectrometer at Menlo Park. Analytical precision for zircon $^{206}Pb^*/^{238}U$ and $^{207}Pb^*/^{235}U$ is ± 1% (2σ). Dates and uncertainties were calculated according to procedures described by Ludwig (1980). Common Pb correction for the diorite was obtained from the mean

composition of feldspar Pb from several sampled Mesozoic plutons from the Granite Mountains and adjacent ranges (Wooden et al. 1988). The mean values are $^{206}Pb/^{204}Pb = 18.34$, $^{207}Pb/^{204}Pb = 15.63$, and $^{208}Pb/^{204}Pb = 39.00$.

Lithologies and ages of plutons

Granite Mountains

Coarse to medium-grained biotite-hornblende diorites and quartz diorites from the Granite Mountains comprise the most voluminous of the Bristol Lake mafic plutons and are the primary focus of this study (Fig. 1). Two non-magnetic zircon fractions from the Granite Mountains pluton were analyzed. The larger fraction (+ 102 μm) is low in U (207 ppm) and is internally concordant, yielding a date of 155 Ma (Table 1, Fig. 2). The smaller size fraction (− 63 μm) is richer in U (513 ppm) and is internally discordant (Fig. 2), yielding $^{206}Pb^*/^{238}U$ and $^{207}Pb^*/^{235}U$ dates of 149.7 ± 0.2 and 151.2 ± 0.5 Ma, respectively (Table 1). The $^{207}Pb^*/^{206}Pb^*$ date of 175.2 ± 7.6 Ma indicates that discordancy in the U-rich zircons is the result of both Pb loss and a minor component of inheritance. The low U concentration of the + 102 μm concordant fraction indicates that loss of Pb in these zircons was negligible. The 155 Ma concordant date is therefore indicative of the crystallization age.

The complete suite spans from hornblende gabbro to granodiorite (I.U.G.S classification of Streckeisen 1976) but diorites predominate. Mutually intrusive relationships between coarser-grained diorite and microdiorite are characteristic and the suite as a whole comprises an autolithic migma. All samples with the exception of GR-002 (Table 1) were collected from the Bull Canyon localities (Fig. 1) on the western side of the range. GR-002 is a partially sheared sample mineralogically similar to the Bull Canyon diorites exposed on the eastern side of the range near Cottonwood Wash.

All of the diorites consist of Pl (plagioclase) + Hbl (hornblende) + Bt (biotite) + Qtz (quartz) + Kfs (K-feldspar) in approximate descending order of abundance (mineral abbreviations after Kretz 1983). Accessory phases include Cpx (clinopyroxene) + Spn (sphene) + Ap (apatite) + Fe-Ti Spl (spinel) + Zrn (zircon). Secondary minerals include trace abundances of uralitic amphibole, chlorite, epidote, and granular sphene. Plagioclase and hornblende form a subophitic-like texture in coarse-grained diorites, indicating simultaneous crystallization early in the subliquidus history. Apatite and zircon occur as large interstitial subhedra and euhedra and rarely as inclusions in biotite, suggesting late-stage crystallization.

Clinopyroxene is found as sparse inclusions in hornblendes of the more mafic samples. Inclusions of clinopyroxene in quartz grains which are in turn poikilitically enclosed in hornblende cores are visible in electron backscatter images (Young 1990). A complete description of the mineral chemistry and conditions of emplacement of the diorites from the Granite Mountains is given by Young (1990).

Bristol Mountains

Medium to fine-grained biotite-hornblende dioritic rocks petrographically similar to those in the Granite Mountains are exposed in the nearby southern Bristol Mountains (Fig. 1). Fox and Miller (1990) have described the petrography, geological setting, and whole-rock geochemistry of these rocks and inferred a Middle to Late Jurassic crystallization age. The Bristol Mountains mafic plutonic suite differs from that in the Granite Mountains by its greater clinopyroxene content. In addition, the Bristol Mountains diorites are intermingled with contemporaneous felsic plutons and have been locally extensively albitized (Fox and Miller 1990). Samples collected for this study contain more secondary chlorite than the Granite Mountains diorites but lack obvious minerological signs of albitization. A single sample from the northern Bristol Mountains (sample NBR-001) is a biotite-hornblende diorite xenolith collected from within a Late Cretaceous (?) granodiorite pluton (Fig. 1).

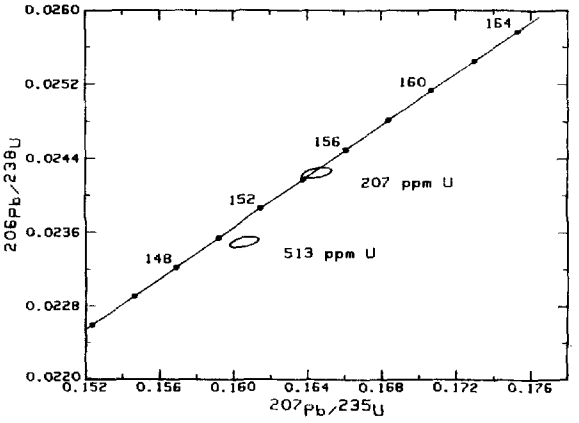

Fig. 2. Concordia plot of zircon fractions from diorite sample GR-036. Error ellipses depict 2σ uncertainties

Providence Mountains

Miller et al. (1985) and Fox and Miller (1990) described medium-grained biotite-hornblende dioritic rocks exposed in the southern Providence Mountains (Fig. 1). The diorites are spatially related to Middle Jurassic felsic intrusives, but their precise crystallization age is now known. Thin sections from the pluton were examined as part of this study but no additional data have been collected to date.

Composition characteristics

Major-element data from this study (Table 2, Fig. 3) and from Fox and Miller (1990) demonstrate that the major-element compositions of the diorite plutons from the Bristol, Granite, and Providence Mountains are broadly similar. Multiple discriminant analysis (MDA, see Le Maitre 1982) was used quantitatively to assess the degree of compositional similarity of the plutons. Discriminant functions consist of $N - 1$ (N is the number of

Table 1. U-Pb isotopic data for sample GR-036 zircons

Fraction	U ppm	Pb ppm	$^{206}Pb^*/^{238}U$	Date (Ma)[a]	$^{207}Pb^*/^{235}U$	Date (Ma)[b]	$^{207}Pb^*/^{206}Pb^*$	Date (Ma)
− 63	513.2	14.0	0.0234903	149.7 ± 0.2	0.160574	151.2 ± 0.5	0.0495777	175.2 ± 7.6
+ 102	207.3	6.0	0.0242445	154.4 ± 0.2	0.164514	154.7 ± 0.5	0.0492139	158.0 ± 7.3

[a] $\lambda(^{238}U) = 1.55125 \times 10^{-10}\,year^{-1}$
[b] $\lambda(^{235}U) = 9.8485 \times 10^{-10}\,year^{-1}$
[c] Pb* = radiogenic Pb

Table 2. X-ray fluorescence analyses of diorites from the Bristol and Granite Mountains

Sample	GR002[b]	GR006[a]	GR016[a]	GR022[a]	GR032[a]	GR035[a]	GR036[a]	GR004[c]	GR007[c]	GR009[c]	NBR001[d]	BR001[e]	BR002[e]
Weight per cent oxides													
SiO_2	49.46	58.23	58.15	52.97	50.19	59.76	49.08	53.04	58.90	51.28	50.28	49.70	49.83
TiO_2	1.60	0.94	1.25	1.03	0.98	1.04	1.23	1.22	0.95	1.34	1.49	1.51	1.48
Al_2O_3	17.92	16.31	17.04	18.20	17.77	18.96	16.67	17.16	17.72	18.14	16.86	16.74	16.93
FeO	10.22	7.41	6.42	7.76	8.13	7.52	9.85	8.33	5.35	9.03	9.34	9.42	9.34
MgO	4.23	3.00	2.70	4.67	5.97	4.69	5.74	4.76	2.59	4.44	5.43	5.78	6.05
MnO	0.14	0.14	0.14	0.14	0.14	0.14	0.16	0.15	0.14	0.17	0.15	0.16	0.17
CaO	10.22	6.06	5.19	7.46	10.31	11.20	11.34	7.54	5.79	8.02	8.95	9.14	9.23
Na_2O	4.09	3.27	3.88	3.63	3.13	3.18	2.82	3.25	4.28	3.75	3.33	2.75	2.91
K_2O	0.33	3.08	2.83	1.88	1.05	0.90	0.95	2.01	2.18	1.59	1.43	1.64	1.45
P_2O_5	0.26	0.35	0.68	0.37	0.24	0.28	0.14	0.42	0.29	0.37	0.23	0.40	0.36
LO_1	0.65	0.68	1.22	1.29	1.44	0.81	1.23	1.31	1.47	1.00	1.75	1.89	1.74
Total	99.12	99.46	99.48	99.39	99.33	99.49	99.22	99.18	99.64	99.40	99.24	99.12	99.50
Parts per million													
Rb	5	102	62	45	31	18	20	70	49	43	57	61	45
Sr	811	557	685	852	711	782	707	627	845	655	498	562	553
Ba	181	1,198	1,793	1,496	289	361	322	1,076	1,132	840	608	623	1,113
Ga	22	19	20	20	18	19	19	19	23	21	19	19	18
Y	26.3	31	43.1	30.1	25.5	24.6	25.9	34.2	14.8	31.3	27.5	32.5	31.9
La	34	60	82	50	19	25	19	53	29	28	21	32	34
Zr	262	242	315	212	98	128	81	226	185	171	101	159	143
Hf	6.6	5.6	7.7	4.9	–	3.4	–	4.7	4.5	4.2	–	–	–
Nb	10.3	18.1	19.1	13.7	11.0	10.2	10.5	16.6	9.5	14.1	13	14.3	13.4
Cr	41	22	20	71	134	122	96	89	15	15	103	119	117
Ni	31	27	6	51	68	45	54	49	9	12	45	48	58
Th		9.3	7.0	–	2.9	–	–	4.1	6.1	3.5	–	5.3	4.2
Pb	9	19	16	13	11	12	11	14	12	10	10	11	10

– Indicates below detection limit
[a] Bull Canyon coarse-grained diorite, Granite Mountains
[b] Eastern Granite Mountains coarse-grained diorite
[c] Bull Canyon microdiorites, Granite Mountains
[d] Northern Bristol Mountains
[e] Bristol Mountains

groups) eigenvectors derived from sums-of-squares matrices such that the ratio of the inter-group to the intra-group mean sum of squares is maximized. As part of the MDA analysis Rao's R statistic was used to test the null hypothesis that the groups of diorite major-element analyses from the three ranges are samples of the same population. A value of R greater than the F statistic indicates that the groups represent distinct populations at the specified confidence level. In this case the null hypothesis is rejected. The strength of the evidence against the null must be evaluated, because rejection of the null does not prove that the populations are distinct (Bhattacharyya and Johnson 1977, p. 179).

Separation among the data for the three diorite plutonic suites is evident from MDA. The resulting R value of 3.68 is slightly greater than the value of 2.10 for F at the 95% confidence level for these data (i.e., the significance probability is near 5%), indicating that the major-element compositions of the three plutons are different at this confidence level. We interpret the 5% significance probability as evidence that the separation among the three groups is not large, however. Justification for this interpretation and further evidence against large differences in major-element chemistry comes from a χ^2 test (see Le Maitre 1982, p. 153 for explanations) which shows that one of the two discriminant functions is statistically meaningless. The MDA results show that the diorite plutons from the Bristol, Granite, and Providence Mountains are similar, but not identical, in their major-element chemistry.

The trace-element data for the Bristol Lake diorites define broadly regular trends when plotted against weight per cent SiO_2 (Fig. 4). Statistical comparison of the trace-element data in Table 2 and those of Fox and Miller (1990) was not performed because the same elements were not analyzed in the two studies and because unknown systematic errors between laboratories are more likely to be important for trace-element data than for major elements. The trends in Fig. 4 are, however, consistent with the results of the major-element statistical test in showing that the Bristol Lake diorites are similar in their elemental concentrations but not identical.

Compositions for the basaltic diorites ($< 53\%$ SiO_2) straddle the CIPW normative enstatite-diopside-albite plane in the basalt tetrahedron, suggesting olivine tholeiite to quartz tholeiite affinities. Leedey chondrite-normalized rare-earth patterns for representative samples from the Granite Mountains pluton are similar to high-alumina basalts from the Aleutian arc (Kay et al. 1982) and high-K andesites (Gill 1981), having steeply negative

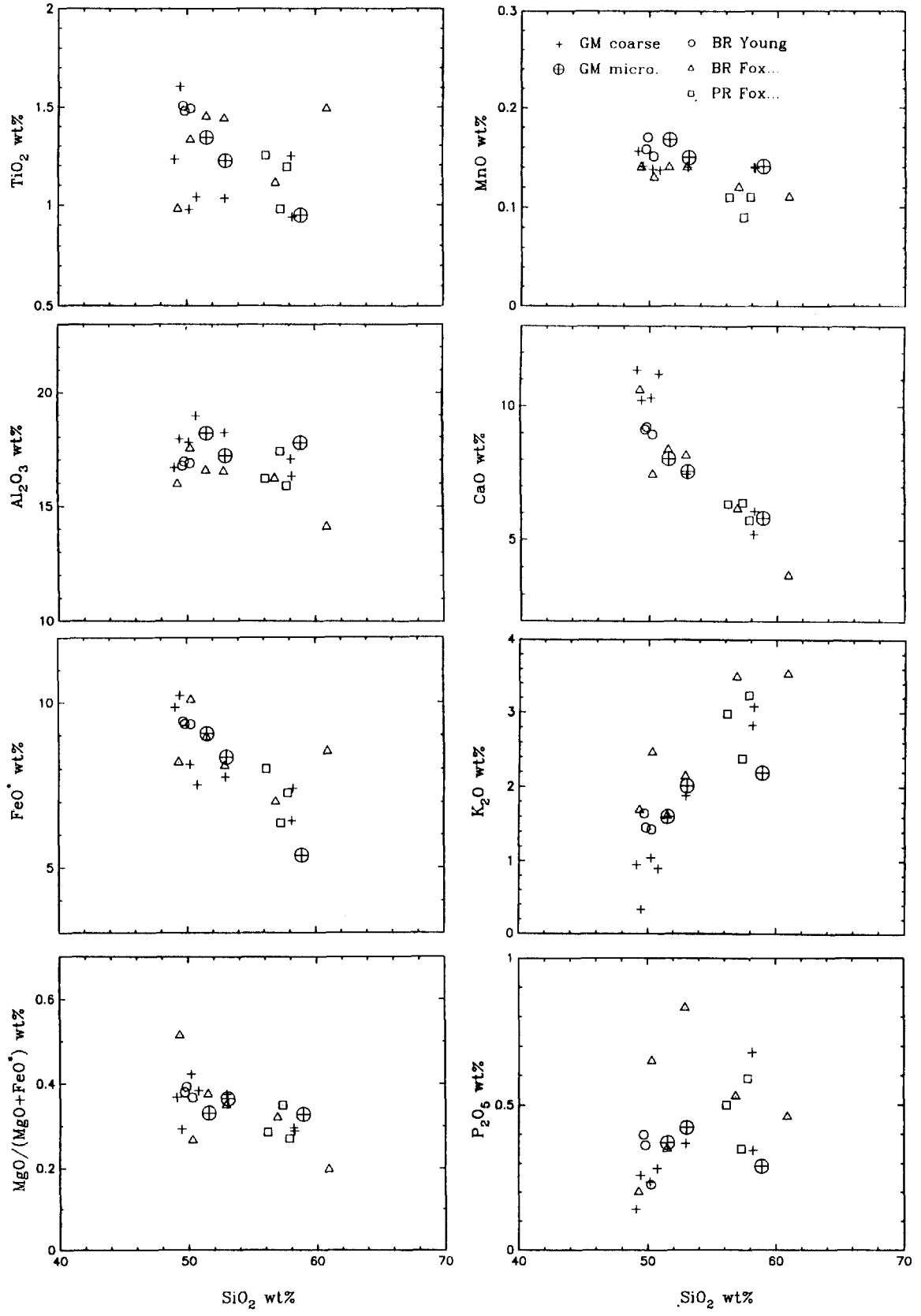

Fig. 3. Major-element variation diagrams for Jurassic diorites from the Bristol Lake region. Symbols are: *GM coarse*, data for coarse-grained dioritic rocks from the Granite Mountains: *GM micro*, data for microdiorites from the Granite Mountains; *BR Young*, data for dioritic rocks from the Bristol Mountains from this study; *BR Fox. . .*, data for dioritic rocks from the Bristol Mountains taken from Fox and Miller (1990); *PR Fox. . .*, data for dioritic rocks from the southern Providence Mountains taken from Fox and Miller (1990)

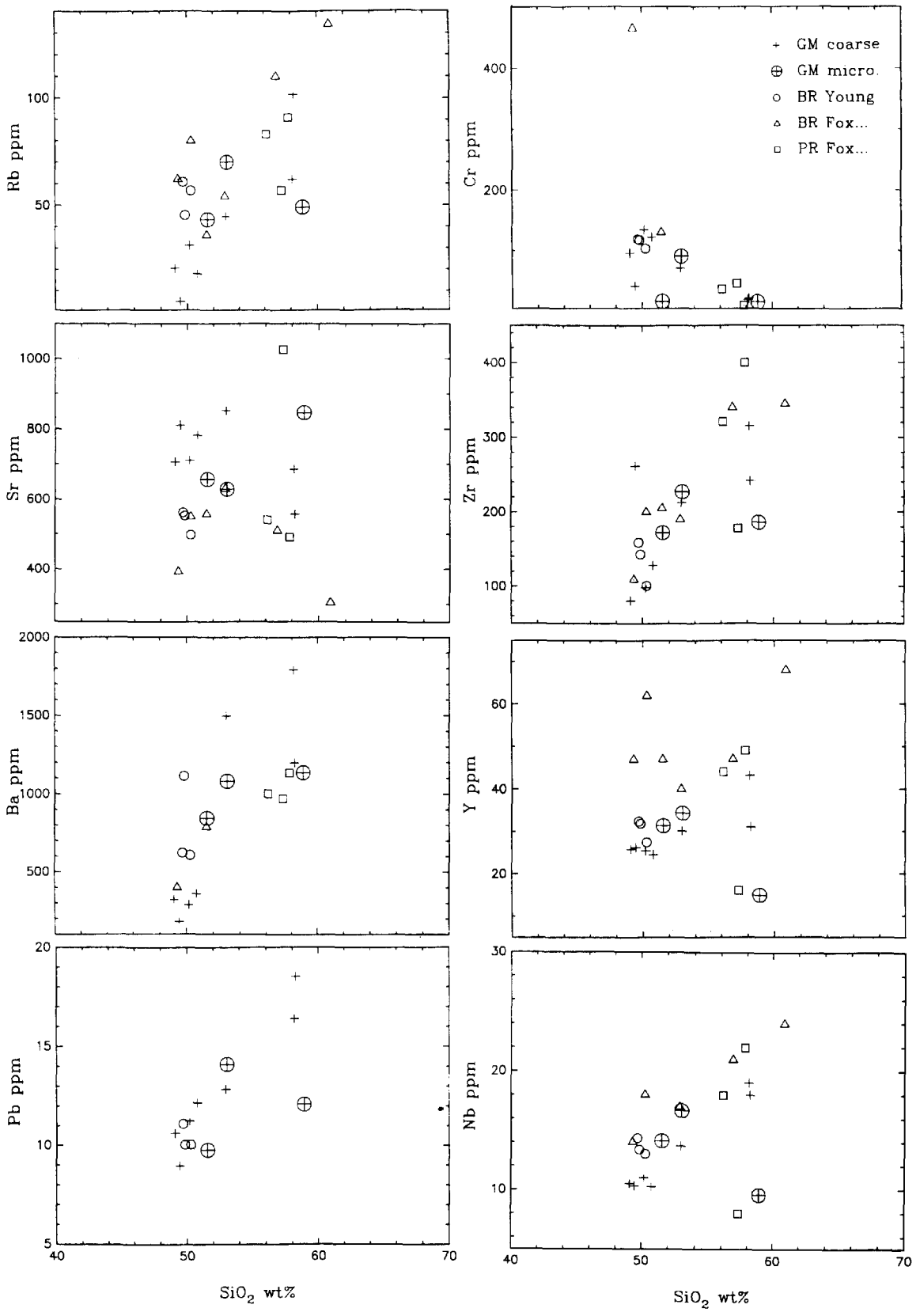

Fig. 4. Trace-element variation diagrams for Jurassic diorites from the Bristol Lake region. Symbols and sources of data are the same as in Fig. 3

slopes for LREE (light-rare-earth elements) and flat slopes for H (heavy) REE (Fig. 5). The average compositions of the basaltic diorites are similar to high-alumina basalts but have higher La, Zr, Nb, and Th concentrations than average Aleutian high-alumina basalt (HAB of Brophy and Marsh 1986). Elevated high-field-strength-element (HFSE) concentrations relative to oceanic basalts ally the basaltic diorites with continental hawaiite basalts (transitional alkali-tholeiites) found in Cenozoic volcanic fields of southern Nevada and continental volcanic arcs worldwide (Fig. 6; Vaniman et al. 1982; Farmer et al. 1989). The andesitic diorites are similar to high-K basaltic andesite but the average is higher in large-ion-lithophile elements (LILE), HFSE, Cr, Ni, and K, and lower in Ca than average high-K basaltic andesite defined by Gill (1981). The elevated HFSE abundances in the diorites are consistent with their high alkali contents (Pearce and Norry 1979). Fomation of alkali-HFSE-silicate complexes may have contributed to the elevated HFSE in the diorites and late crystallization of zircon by increasing the solubility of HFSE-rich phases (Collins et al. 1982).

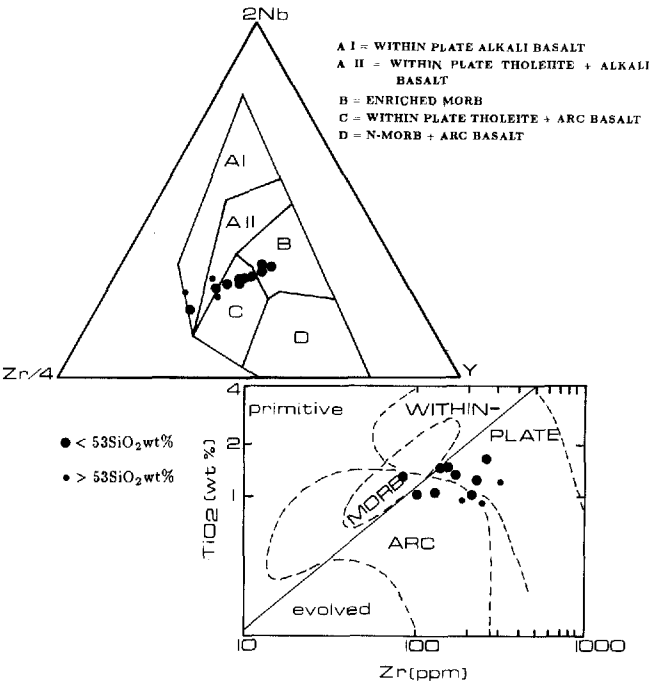

Fig. 6. Whole-rock compositions of Granite Mountains diorites plotted on the basalt discrimination diagrams of Pharaoh and Pearce (1984) (TiO_2 versus Zr) and Meschede (1986) (Nb-Zr-Y)

Pearce element ratio analysis

Theory

Pearce element ratios (Russell and Nicholls 1988; Ernst et al. 1988; Nicholls 1988; Pearce 1968) were used to determine which, if any, of the compositionally similar diorites from the Bristol Lake region are comagmatic and to elucidate the causes of the trends in Figs. 3 and 4.

Pearce element ratios are cation ratios in which a conserved element, Z, is the denominator. The conserved element for a suite of rocks is one for which the absolute abundance (extensive quantity) remained the same throughout the processes responsible for the variations in chemical composition. In the case of differentiation by crystallization, Z would be an incompatible element with a bulk partition coefficient less than approximately 0.1 (Ernst et al. 1988). Formulated in this fashion, Pearce element ratios are free from both the spurious correlations induced by formation of ratios and correlations produced by the closure inherent in weight-fraction data (see Chayes 1971).

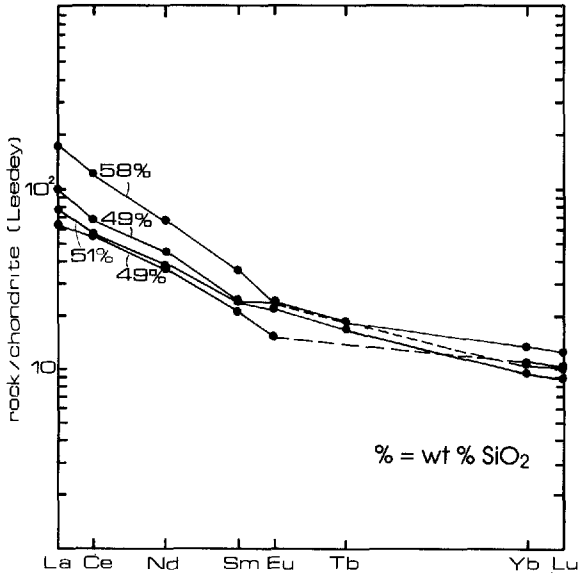

Fig. 5. Leedey chondrite-normalized REE abundances of four samples of diorite from the Granite Mountains. Note increase in Σ REE with increasing weight per cent SiO_2

Ernst et al. (1988) advocate normalizing Pearce element ratios by multiplying by the molecular proportion of the Z element in a reference sample (Z_o). A corollary of this procedure is prescribed by the equation:

$$Z_o/Z_i = (Z_o^*/T_o^*)(T_i^*/Z_i^*)$$
$$= (T_i^*/T_o^*) \quad \text{for } Z_i^* = Z_o^* \qquad (1)$$

where Z_i is the molecular proportion of the conserved element Z for the ith sample, the star symbol designates absolute quantities, and T_i^* and T_o^* are the total weights of sample i and the reference sample, respectively. Equation 1 shows that the ratio Z_o/Z_i is numerically equivalent to the weight fraction of sample i relative to the reference sample when the element Z is conserved. When the reference sample is chosen as the most primitive sample in a suite or rocks representing liquids related by differentiation, Z_o/Z_i is equivalent to the F parameter used in trace-element modeling (cf. Minister et al. 1977, Eq. 6). Equation 1 was used in this study to compare estimates of F obtained from Pearce element ratios to values derived from trace-element modeling, providing a measure of internal consistency.

Comagmatic tests

The 95% confidence interval for non-zero intercepts on all Pearce element ratio plots of geochemically distinct numerators with P as the denominator (e.g., Fig. 7) indicate that P was a conserved element during differentiation of the Bristol Lake diorite magmas (Nicholls 1988). Restriction of Ap crystallization to late stages, as suggested by its interstitial occurrence, explains the conservation of P. Plots analogous to Fig. 7 using Hf, Zr, and La show that these elements were also largely conserved and are consistent with petrographic observations suggesting late-stage crystallization of Zrn and Ap. The ratios Hf : P and La : P for diorites from the Granite Mountains and Bristol Mountains are constant within 3σ uncertainties. Statistical overlap among the conserved element ratios is consistent with derivation of the Bristol and Granite Mountains diorites from similar parental magmas (Russell and Nicholls 1988).

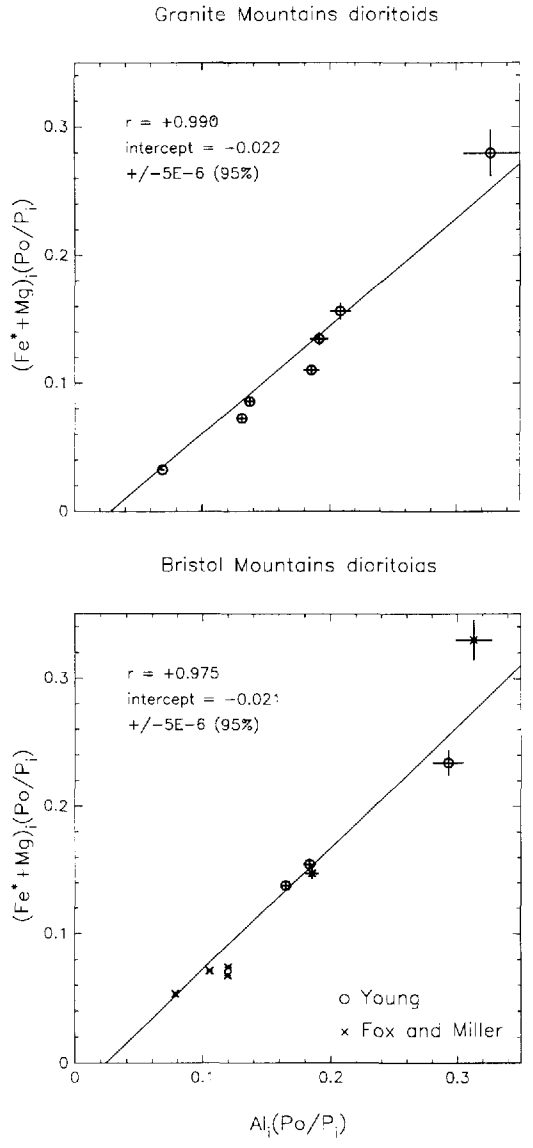

Fig. 7. Normalized Pearce element ratio plots of diorite whole-rock compositions from the Granite and Bristol Mountains. The Bristol Mountains plot includes data from Fox and Miller (1990). Error bars indicate 3σ precision uncertainties in analyses. Note statistically significant non-zero intercepts of best-fit lines

Differentiation trends

Variations in major-element concentrations in igneous rocks are reflected in variable modes irrespective of the specific differentiation processes involved. Pearce element ratios were employed to elucidate the degree to which different minerals contributed to the observed chemical trends in the Granite Mountains diorites. Linear combinations of cation variables were used to construct numerators corresponding to specific mineral stoichiometries (complex numerators of Ernst et al. 1988) for this purpose. Pearce element ratio data transformed into complex numerators are proportional to absolute molar abundances of phases relative to the initial mass T_0^* (cf. Eq. 1). Numerators corresponding to phases involved in the differentiation process should correlate significantly with one another and F.

The abundant Hbl in the diorites required formulation of complex numerators specific to this study. The P : K cation ratios for all but one of the samples of the suite are identical within 3σ uncertainties and the anomalous sample deviates only slightly from the others (3.1σ), indicating that K was nearly conserved. Therefore, addition or subtraction of the K-rich phases Bt and Kfs could not have been important in determining the chemical variability of the diorites. Since Bt, Kfs, Zrn, and Ap crystallized late in the paragenetic sequence and did not contribute to the differentiation of the diorites, it is also unlikely that late-crystallizing quartz (an interstitial phase) could have been an important factor. The remaining phases which may have influenced the composition trends are Hbl, Cpx, Pl, and Spn. Linearly independent variables representing molar abundances of Hbl, Cpx, Pl, and Spn, were computed from the variables (Ca + Na), (Fe + Mg), (Si + Al), and Ti using standard linear algebraic techniques. Sums of geochemically similar cations were used as variables to reduce the influence of variations in phase composition on the results. Mineral compositions were taken from average microprobe analyses collected from representative samples of Granite Mountains diorite (Young 1990).

Strong correlations between Hbl, Pl, and F computed from Eq. 1 suggest that both phases were likely to have been important factors in the differentiation process (Fig. 8). Sample Gr-036 was used as the reference sample for computing F based on its primitive composition (Table 2). No correlation between Spn and F is evident in the data. The data yield a poor correlation between Cpx and F but this result was shown to be inconclusive because the relative influences of Hbl and Cpx are not easily distinguished using Pearce element ratios. This ambiguity was demonstrated by testing the reliability of the norm transformation on fictive random dioritic rock compositions generated with algorithms similar to those described by Nicholls (1988). Fictive compositions were generated by randomly varying the modal proportions of Cpx or Hbl, Pl, Kfs, Qtz, Bt Spl, and Spn. Limits on the ranges in modal proportions were set to correspond with typical

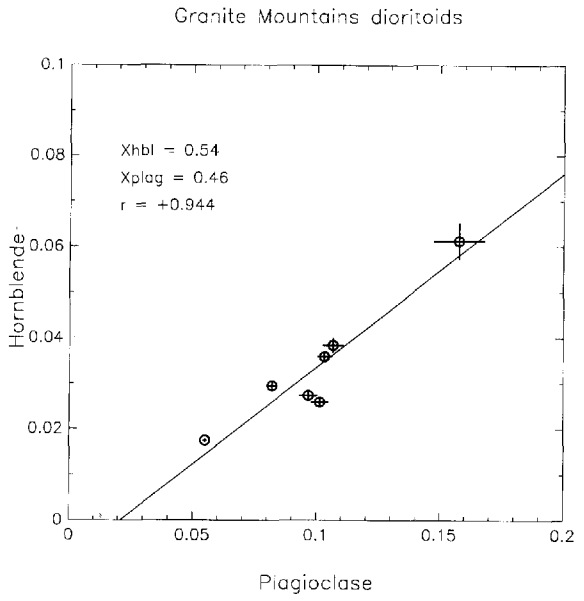

Fig. 8. Pearce element ratio plot of Granite Mountains coarse-grained diorites illustrating the importance of plagioclase and hornblende in influencing whole-rock compositions. The Plagioclase and Hornblende axes are proportional to the moles of plagioclase and hornblende, respectively, for each sample relative to the initial mass of the system. The variables are: Plagioclase = 0.277 (Si + Al) − 0.447 (Fe + Mg) − 0.106 (Ca + Na) − 0.170 (Ti); Hornblende = 0.106 (Si + Al) + 0.213 (Fe + Mg) − 0.426 (Ca + Na) + 0.319 (Ti). Derivation of these parameters is described in the text. X_{hbl} and X_{plag} are the weight fractions of Hbl and Pl derived from the slope of the best-fit line through the data, *solid line* (see text)

dioritic rocks. The absolute quantity of Ap was held constant (but not the modal proportion) to simulate conservation of P. The norm transformation applied to the fictive data showed that the complex numerators used in this study are effective in discriminating among the relative importance of Pl, Hbl, and Spn of variable composition. However, the tests showed that the effects of variations in Hbl and Cpx could not be reliably distinguished.

The molar Hbl/Pl ratio involved in the differentiation of the Granite Mountains diorite magma is given by the slope of the best-fit line in Fig. 8 (see Ernst et al. 1988, for a discussion). After correction for specific gravities and molar volumes, the slope in Fig. 8 yields weight fractions of Hbl and Pl of 0.54 and 0.46, respectively.

Fractional crystallization inverse models

Correlations on Pearce element ratio diagrams show that the diorite samples from the Granite Mountains are related, but the process of differentiation is not revealed. Steeply negative linear trends in log Cr-log Hf diagrams and analogous plots of compatible (ordinate) and incompatible (abscissa) elements suggest that fractional crystallization was the dominant differentiation process (Cocherie 1986). The steep linear trends require that the rocks comprise either the solid cumulates or the solidified liquids produced during fractional crystallization. The data are not consistent with significant mixing between solid residue and liquid because on such log-log plots gently sloping curves convex away from the ordinate would result from this process (e.g., Fig. 1 of Cocherie 1986). Since there is no clear field or petrographic evidence that the rocks are dominated by cumulates (e.g., primary layering), we conclude that their compositions are representative, albeit imperfect, of liquids related by fractional crystallization. Accordingly, models presented below which describe the fractional crystallization process rely upon whole-rock elemental concentrations as estimates of liquid compositions. Errors attributable to deviations from liquid compositions typical of plutonic rocks were reduced by modeling many elements simultaneously and including average rock compositions in the calculations.

Inverse modeling of the fractional crystallization process relating the Granite Mountains samples was used to derive the possible weight fractions of fractionating solids and the weight fractions of melt represented by each sample. The results of the models based on trace elements are in rough agreement with the results of the major-element Pearce element ratio analysis.

The familiar equation for perfect fractional crystallization is:

$$C_l^j = C_o^j F^{D_o^j - 1} \tag{2}$$

where C_l^j is the concentration of element j in the fractionated liquid, C_o^j is the concentration in the original liquid, F is the weight fraction of liquid remaining, and D_o^j is the bulk distribution coefficient for element j. Barca et al. (1988) noted that F and D_o^j are not independent parameters. They reformulated Eq. 2, yielding:

$$C_l^j = C_o^j \left(1 - \sum_i y_i\right)^{(\Sigma_i y_i K_{i,j}/\Sigma_i y_i - 1)} \tag{3}$$

where F has been replaced by $1 - \Sigma_i y_i$, y_i is the mass of phase i in the fractionating solid relative to the initial mass, and $K_{i,j}$ is the solid-liquid partition coefficient of element j for solid i. The F and the bulk distribution coefficient are related through the y_i terms. The reformulation of Barca et al. permits simultaneous solution for both the mass fraction of liquid and the mass fractions of the fractionating minerals given $K_{i,j}$ and C_l^j/C_o^j for numerous elements. Use of multiple elements in this fashion reduces the influence of individual partition coefficients and compensates for random deviations from pure liquid compositions. As in any trace-element modeling, the significant uncertainties in partition coefficients limits the accuracy of the results.

Inverse modeling based on Eq. 3 is a standard optimization problem in which the parameter to be minimized is:

$$\psi(X) = 1/2 \sum_j (f_j(X))^2 \tag{4}$$

where $f_j(X)$ is given by

$$f_j = C_o^j \left(1 - \sum_i y_i\right)^{(\Sigma_i y_i K_{i,j}/\Sigma_i y_i - 1)} - C_l^j \tag{5}$$

and X is the vector $[y_1, y_2, \ldots]$. The Levenberg-Marquardt descent method (Marquardt 1963) was used in this study to find X corresponding to minimum $\psi(X)$. This algorithm is a modification of a least-squares method

(damped least-squares) which alleviates problems arising from ill-conditioning by treating $\psi(X)$ as a convex function. The derived vector X provides the best estimate of F and the relative masses of fractionating phases capable of explaining the input data.

Total rare-earth abundances (ΣREE) in the diorites increased during differentiation (Fig. 5), indicating that the accessory phases Ap, Zrn, and Spn were not important in the fractionating solid assemblage. The incompatible behavior of P, Zr, Hf, and La during differentiation was demonstrated with Pearce element ratio analysis and supports this conclusion. For these reasons, the accessory phases were not included in the optimization modeling.

Various combinations of REE, LILE, and HFSE were subjected to optimization. Preferred partition coefficients used in this study are listed in Table 3. Partition coefficients were taken from the literature and reflect intermediate and basaltic bulk compositions. Best-fit solutions using pairs of rocks (Table 4) were obtained using sample GR-036 as the common parental melt. GR-036 is the least evolved of the sampled diorites from the Granite Mountains. Models failed to converge when Bt was included as a fractionating phase, in agreement with the results of the Pearce element ratio analysis. Assemblages composed of Pl + Hbl or Pl + Cpx yielded the best solutions (e.g., Table 4). Lack of convergence in some models based on Pl + Cpx and generally higher sums of squared errors relative to models based on Pl + Hbl favor hornblende over pyroxene as the dominant fractionating mafic phase. Optimal solutions for each rock pair suggest fractionation of approximately 0.7 to 0.8 weight fraction of Hbl (X_{Hbl}) in the assemblage Pl + Hbl (Table 4). An average optimal fractional crystallization model based on REE, LILE, and HFSE was computed using the mean composition of the basaltic members of the diorite suite as the parent and the mean of the andesitic members as the derivative melt (Table 4). Average compositions reduce the dependence of the results on deviations from liquid compositions by individual rocks. The results of the average model give an X_{Hbl} of 0.66 in the assemblage Pl + Hbl, and an F of 0.34. The indicated ratio of Hbl to Pl is similar to that derived from Pearce element ratios (cf. Fig. 8).

Table 3. Solid/liquid partition coefficients used in model calculations

Element	Bt	Hbl	Cpx	Pl[a]
La	0.03	0.27	0.08	0.14
Ce	0.04	0.34	0.34	0.14
Nd	0.03	0.19	0.60	0.08
Sm	0.03	0.91	0.90	0.08
Eu	0.03	1.0	0.90	0.32
Yb	0.18	0.97	1.0	0.07
Lu	0.04	0.89	0.84	0.08
Rb	3.3	0.25	0.04	0.10
Sr	0.12	0.57	0.14	1.8
Ba	6.4	0.31	0.07	0.23
Zr	0.60	0.50	0.10	0.01
Y	0.03	1.0	0.50	0.03
Nb	1.0	0.80	1.10	0.01

[a] Sources: Henderson (1982); Nicholls and Harris (1980); Pearce and Norry (1979)

The bulk distribution coefficients for Zr and La for the average model are 0.33 and 0.22, respectively. Pearce element ratios described above suggest that these elements were conserved (i.e., they were highly incompatible). The deviations from perfectly incompatible behavior implied by the model D_o would impart errors on the order of 30% (at intermediate values for F) to Pearce numbers calculated with Zr or La as the Z element (Ernst et al. 1988).

Rare-earth elements yielded the largest F values for each sample relative to GR-306, HFSE gave intermediate F values, and LILE + REE indicated the smallest F values. The different element groups produced total ranges in F on the order of 0.2 per rock pair. The F values for

Table 4. Optimum fractional crystallization model results based on La, Rb, Sr, Ba, Zr, Nb, and Y for selected samples from Table 2 and the average Granite Mountains basaltic and andesitic diorite compositions

	Parent	Individual sample models[a] Model differentiates						Average model[b] Parent	Model differentiate
	GR-036	GR-035	GR-032	GR-022	GR-006	GR-016	GR-002	< 53% SiO_2	> 53% SiO_2
La[c]	19	18 (25)	12 (19)	59 (50)	75 (60)	49 (82)	16 (34)	22	51 (56)
Rb	20	50 (18)	32 (31)	65 (45)	83 (102)	137 (62)	42 (5)	29	68 (82)
Sr	707	318 (782)	838 (711)	1,030 (852)	906 (557)	1,184 (685)	743 (811)	763	770 (621)
Ba	322	697 (361)	490 (289)	930 (1,496)	1,143 (1,198)	1,808 (1,793)	621 (181)	617	1,345 (1,496)
Zr	81	217 (128)	112 (98)	191 (212)	242 (242)	339 (315)	146 (262)	130	268 (278)
Nb	10	4 (10)	13 (11)	21 (14)	24 (18)	16 (19)	16 (10)	11	19 (19)
Y	26	68 (25)	28 (26)	32 (30)	39 (31)	39 (43)	34 (26)	27	38 (37)
x^d_{Hbl}	–	1.0	0.88	0.85	0.76	0.82	0.70	–	0.66
x_{Pl}	–	0.0	0.12	0.15	0.24	0.18	0.30	–	0.34
F	1.0	0.34	0.55	0.22	0.17	0.10	0.40	1.0	0.34

[a] Liquid compositions representing the best fit to indicated rock samples
Numbers in parentheses are measured sample values from Table 2
[b] Liquid composition representing best fit to average Granite Mountains diorites with SiO_2 > 53 wt% (model differentiates) based on a parent of average granite Mountains diorite with SiO_2 < 53 wt% (parent). Parentheses give actual average values for comparison with model
[c] Concentrations in parts per million
[d] Weight fractions in fractionating solid assemblage

the seven coarse-grained diorite samples obtained by optimization of the elements Sr, Rb, Ba, Zr, Y, Nb, and La, and the F values for the same samples obtained from Pearce element ratio analysis (i.e., Eq. 1) are compared in Fig. 9. At low F, Pearce element ratios yield systematically higher F values than trace-element modeling by approximately 0.1 to 0.2. The *relative* values of F obtained from the two methods are in agreement, however, as shown by the linear correlation coefficient of 0.98. The correlation in Fig. 9 is striking in view of the abundant sources of uncertainty in the two independent methods used to obtain F.

Rubidium-strontium isotopes

The Sr isotopic data for the mafic plutons from the Granite and Bristol Mountains collected as part of this study are presented in Table 5. No data are available for the Providence Mountains diorites. The data show considerable scatter on a Rb-Sr isochron diagram. $(^{87}Sr/^{86}Sr)_i$ of the Granite Mountains coarse-grained diorites from Bull Canyon correlate with all indicators of differentiation (Fig. 10). The microdiorites from the suite generally scatter irregularly about the systematic trends defined by coarse-grained diorites. If the variable initial Sr isotopic ratios in the dioritic rocks were inherited from partial melting of a heterogeneous source, more scatter in isotope ratio-element plots would be expected because multiple parental melts with distinctive differentiation histories would have resulted.

Simple binary mixing produces a linear relationship between $(^{87}Sr/^{86}Sr)$ and 1/Sr. Data for the coarse-grained diorites from the Granite Mountains define a linear array on a $(^{87}Sr/^{86}Sr)_i - 1/Sr$ diagram, suggesting that these data can be explained by two-component mixing. However, the companion-plot method of Langmuir et al. (1978) demonstrates that binary mixing is not the best explanation for covariations in Sr isotopes and elemental abundances in the Granite Mountains data. Plots of the initial Sr isotopic values against elemental ratios should delineate hyperbolic curves with curvatures defined by the ratio of the denominators if simple binary mixing applies. These same data will define a straight line when the isotope ratio and the ratio of the denominators from the original plot are used as axes. The Granite Mountains data define non-linear smooth curves on companion plots. For example, only 67% (corresponding to a linear correlation coefficient of 0.83) of the variability between $(^{87}Sr/^{86}Sr)_i$ and $Zr/^{86}Sr$ can be explained by a linear relationship. The correlation coefficient is significant, judging from comparison with the null correlation coefficient of 0.12 (calculated according to Chayes 1971), but is not sufficiently high to be consistent with simple mixing alone. Moreover, simple mixing between end-members represented by pairs of diorite samples produces virtually straight lines in elemental-isotope ratio diagrams in contrast to the observed curved trends (Fig. 10), and petrographic evidence indicative of magma mixing (e.g., normally and reversely zoned crystals of a single mineral, cf. Wyers and Barton 1989) is not present in the dioritic rocks.

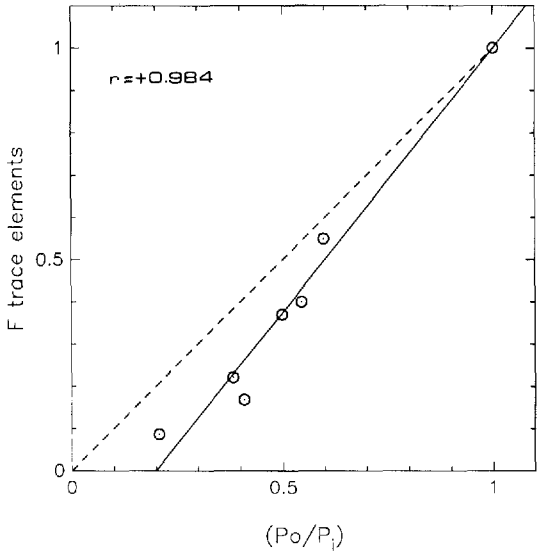

Fig. 9. Comparison of relative weight fractions of magma represented by samples of coarse-grained diorite from the Granite Mountains derived from trace-element models of fractional crystallization and Pearce elemental ratios (Eq. 1). *Dashed line* shows 1 to 1 correlation. *Solid line* illustrates linear regression

Table 5. Sr isotope data for Bristol Lake diorites

Sample	Rb/Sr[a]	$^{87}Rb/^{86}Sr$	$(^{87}Sr/^{86}Sr)_{meas}$	Age (Ma)	$(^{87}Sr/^{86}Sr)_i$[b]
GR-036	0.0289	0.0836	0.70704	155	0.70686
GR-035	0.0229	0.0663	0.70764	155	0.70749
GR-032	0.0440	0.1272	0.70765	155	0.70737
GR-022	0.0523	0.1513	0.70817	155	0.70784
GR-016	0.0904	0.2616	0.70876	155	0.70818
GR-002	0.0060	0.0174	0.70779	155	0.70775
GR-009	0.0656	0.1897	0.70726	155	0.70684
GR-007	0.0578	0.1673	0.70885	155	0.70848
GR-004	0.1112	0.3218	0.70830	155	0.70759
BR-001	0.1081	0.3128	0.70889	155	0.70820
BR-002	0.0819	0.2370	0.70863	155	0.70811
NBR-001	0.1141	0.3301	0.70770	155	0.70697

[a] Based on X-ray fluorescence analyses
[b] Initial value based on $\lambda_{Rb} = 1.42 \times 10^{-11}$ year^{-1}

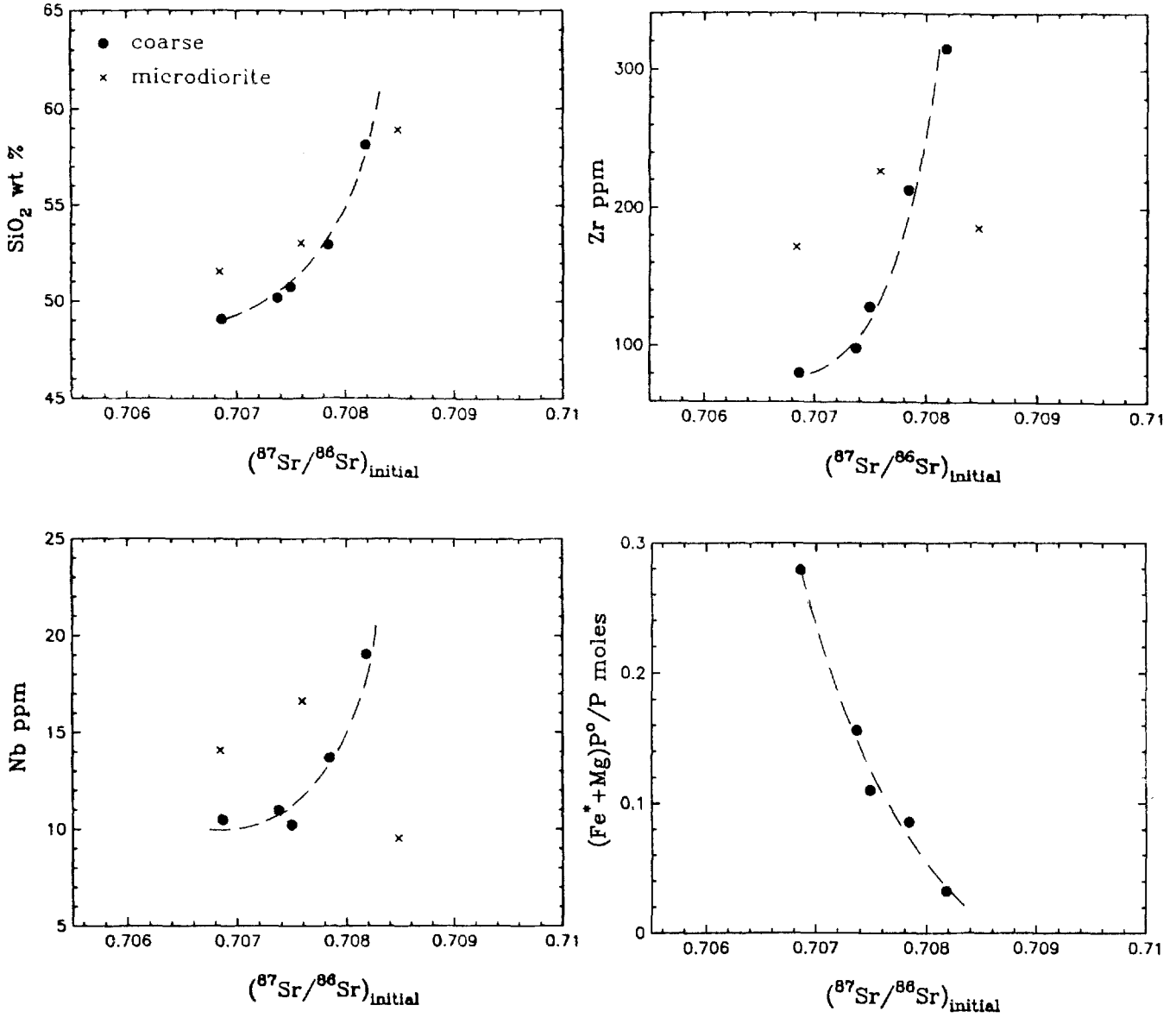

Fig. 10. Concentrations of SiO_2, Zr, Nb, and the normalized Pearce element ratio $(Fe^{total} + Mg)/P$ versus $(^{87}Sr/^{86}Sr)_i$ for the coarse-grained diorites and microdiorites from Bull Canyon, Granite Mountains

The success of the fractional crystallization models in explaining the trace elemental trends of the diorites and the lack of evidence for simple magma mixing suggests that variable $(^{87}Sr/^{86}Sr)_i$ in the Granite Mountains diorite suite is the product of assimilation and fractional crystallization. Because variability in trace-element concentrations can be explained largely by fractional crystallization alone, the extent of assimilation must have been comparatively small.

Assimilation inverse model

In theory, isotope ratios and elemental concentrations of rocks comprising melts related by combined fractional crystallization and assimilation (AFC) can be used to constrain the relative rates of assimilation and crystallization, the average assimilated composition, the composition of the parental melt, and the proportions of possible fractionating minerals. Recovery of this information involves minimization of a function analogous to Eq. 4 where $f_j(X)$, the difference between predicted and observed elemental and isotopic compositions j, are evaluated with AFC model equations (e.g., DePaolo 1981). In practice, solutions which best fit the measured data are difficult to obtain because the AFC model equations are highly nonlinear and include numerous unknown parameters. Gradient-related methods (e.g., the Levenberg-Marquardt method, cf. Minister et al. 1977) when applied to these equations can yield local minima and proving that the answer obtained is the best fit to the data (the global minimum) is difficult. In order to avoid some of these pitfalls, we applied a simple Monte Carlo (iterative random search) technique (Press 1968) to derive the relative

rate of assimilation and contaminant characteristics which best explain the Granite Mountains diorite data.

The AFC model equations of DePaolo (1981) were used in the Monte Carlo calculations to predict magma isotope ratios and element-weight concentrations. Data for samples GR-036 and GR-022 were taken as representative of the parental and evolved melts, respectively. The calculations therefore only model that portion of the magmatic evolution represented by these samples. The fractionating assemblage was assumed to be Pl + Hbl in accord with the major- and trace-element modeling presented above. The unknown parameters to be fitted included the rate ratio of assimilation to crystallization (r), the weight proportions of fractionating Pl and Hbl (X_{Hbl}), the weight fraction of remaining melt (F), the Sr isotopic ratio of the contaminant, and the concentrations of Sr, Rb, La, Y, Ba, Zr, and Nb in the assimilated material. Random draws were made for each parameter and the predicted melt $(^{87}Sr/^{86}Sr)_i$ and elemental concentrations corresponding to these parameters were compared with those of sample GR-022. After a prescribed number of iterations the parameters which produced the best fit to the measured data were returned by the program.

Initially, all of the fit parameters were allowed to vary within physically meaningful yet liberal limits (e.g., $F = 0 - 1$, Sr = 0–4,000 ppm). Since $(^{87}Sr/^{86}Sr)_i$ increases with fractionation in the diorite suite (Fig. 10), the assimilate $^{87}Sr/^{86}Sr$ was constrained to be greater than the maximum diorite value of 0.70848. The bounds defined the feasible space to be searched. After numerous trial Monte Carlo runs the search space could be condensed, resulting in refinements of the solutions and reductions in computer time. For example, all solutions gave proportions of fractionating Pl and Hbl similar to the inverse fractional crystallization models. As a result, the total space to be searched was limited by setting X_{Hbl} equal to 0.66, the value obtained from the trace-element modeling of average compositions. Similarly, the F values derived from fractional crystallization modeling and Pearce element ratios were considered to be *roughly* indicative of the AFC model results because values obtained with the former independent methods agreed to within $\pm$ 0.2 (Fig. 9) and because very large amounts of assimilation required to alter F significantly were deemed unlikely because of the success of the fractional crystallization models. Initial Monte Carlo runs invariably showed that F values within $\pm$ 0.2 of the previously determined values could not be obtained unless the assimilate had $^{87}Sr/^{86}Sr$ less than 0.7200 and Sr concentrations greater than about 1,000 ppm. The search therefore was limited further by adopting 1,000 ppm as the minimum for the assimilate Sr concentration and 0.7110 as the assimilate $^{87}Sr/^{86}Sr$ where the latter represents values between the minimum required by the data and the maximum suggested by trial runs. The limits on feasible assimilate parameters were checked with forward AFC calculations.

The total error (Eq. 4) encountered during one of the Monte Carlo searches is shown in Fig. 11 as a function of r and F. The shape of the error surface is characteristic of all of the searches and shows that the diorite data are not compatible with a high r *together with* a high F. The optimal solution corresponds to an r of 0.10 $\pm$ 0.05 and an

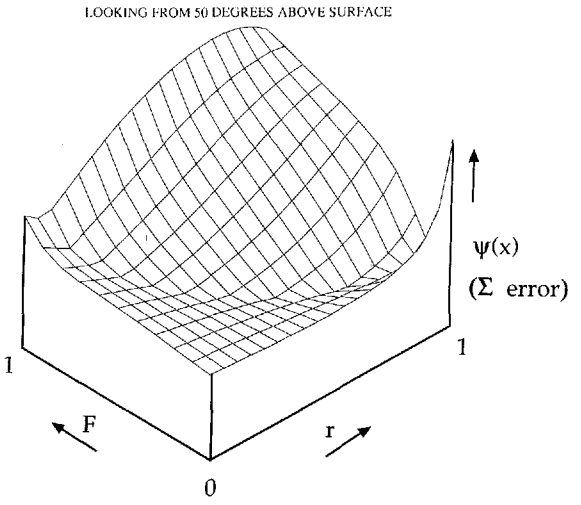

Fig. 11. Perspective view of typical error surface for inverse AFC model discussed in text. Sum of errors $\psi(X)$ is plotted in coordinates of r (rate of assimilation relative to crystallization) and F (weight fraction of remaining magma). Sharp peak near $r = 1$ results from the r − 1 denominator term in the AFC model equation of DePaolo (1981). The shape of the surface demonstrates the incompatibility of high r together with high F in modeling the diorite data

F of 0.30 $\pm$ 0.04 where the uncertainties are 1σ derived from ten searches of the same feasible space. The optimal r and F give a value of 0.08 for the ratio of the mass of assimilate to the mass of parental magma (Farmer and DePaolo 1983).

The AFC inverse model predicts that the assimilated material had the following elemental concentrations: Sr = 1,500 ppm (1,000–1,500 ppm), Rb = 18 ppm (18–200 ppm), La = 20 ppm (20–60 ppm), Y = 6 ppm (1 − 15 ppm), Ba $\geq$ 1,000 ppm (1,000–2,500 ppm), Zr = 200 ppm (80–300 ppm), and Nb = 2 ppm (1–11 ppm). The numbers in parentheses are the ranges for which individual F values, as determined for each element using forward calculations, vary from 0.3 to 0.6 (cf. optimal F of 0.3 and Pearce element ratio F of 0.4). The significant ranges in permissible concentrations illustrate the insensitivity of the calculations to the precise assimilate composition and are the result of broad valleys in the element-error surfaces caused by the low rate of assimilation in the model. The low r and nearly unit Sr bulk distribution coefficient impart the potential for large variations in Sr behavior. For example, the decrease in Sr with $(^{87}Sr/^{86}Sr)_i$ exhibited by the most fractionated sample (GR-016) relative to the model parent, in contrast to the increasing trend defined by the other samples, can be explained by less than 17% more Pl in the fractionating assemblage (Fig. 12). The sensitivity of Sr behavior to Pl/Hbl means that the data in Fig. 12 are adequately explained by either differences in Pl/Hbl occurring persistently throughout fractionation, yielding a range in Sr-$(^{87}Sr/^{86}Sr)_i$ slopes, or changes in Pl/Hbl *during* fractionation, resulting in reversals in Sr-$(^{87}Sr/^{86}Sr)_i$ trends (Fig. 12; cf. DePaolo 1981). The possible origins of the assimilate predicted by these calculations are discussed below following description of the O isotope data.

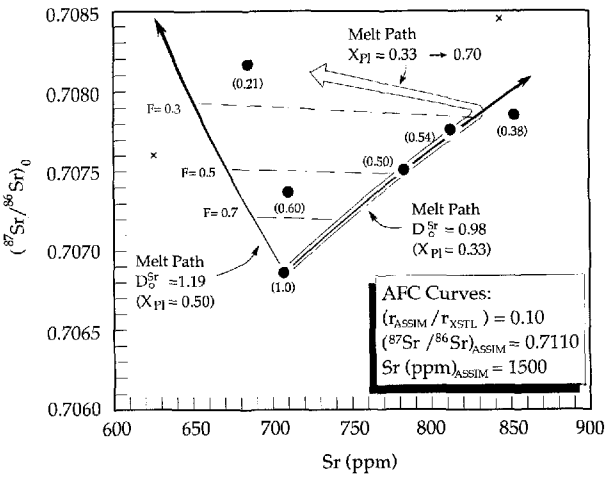

Fig. 12. $(^{87}Sr/^{86}Sr)_i$ vs Sr plot comparing Granite Mountains coarse-grained diorites, *solid circles*; and microdiorites, *crosses*, with AFC melt paths. Rate ratio of assimilation to fractional crystallization (r) and assimilate composition were derived from optimal solutions to the inverse problem described in the text. Numbers in parentheses are F values indicated by Pearce element ratios. Bulk distribution coefficients for Sr (D^{Sr}_o) correspond to the indicated weight fractions of Pl in the fractionating assemblage Pl + Hbl. A two-stage AFC melt path defined by a change in fractionating Pl/Hbl is depicted by the *open arrow*

Oxygen isotopes

Whole-rock $\delta^{18}O$ ($\delta^{18}O^{WR}$) for diorites from Bull Canyon area of the Granite Mountains range from 6.5 to 7.6 per mil. Diorites from the Bristol Mountains and the single diorite sample from the eastern Granite Mountains have lower $\delta^{18}O$ of 4.7 to 5.7 per mil (Table 6). Two samples from the Bristol Mountains are anomalously low relative to typical unaltered igneous rocks. Although the Bristol Mountains samples show no obvious signs of alteration in hand specimen, they generally contain more chlorite (principally after biotite) than the diorites from the Bull Canyon area. This together with the fact that the eastern Granite Mountains rock is deformed leads us to conclude that the low $\delta^{18}O$ values from outside of the Bull Canyon area are the result of interaction with meteoric or evolved meteoric water-rich fluid at moderately high temperatures at the level of emplacement. Fox and Miller (1990) attributed ^{18}O depletion in similar diorites from the Bristol and Providence Mountains to post-magmatic interaction with meteoric water. The single sample of sheared diorite from the eastern Granite Mountains occurs near the Providence Mountains complex and apparently has been similarly affected.

The low $\delta^{18}O$ of the most primitive sample (GR-036) relative to the consistent values of the other diorite samples from Bull Canyon suggests possible enrichment in ^{18}O during differentiation (Fig. 13). Closer scrutiny, however, demonstrates that the lower $\delta^{18}O$ of sample GR-036 is the result of minor subsolidus alteration. Mineral separates from sample GR-036 yield a $\Delta_{Qtz-Hbl}$ ($\delta^{18}O_{Qtz} - \delta^{18}O_{Hbl}$) of 3.5 per mil (Table 6), corresponding to a temperature of $\sim 650°C$ (Bottinga and Javoy 1975). The Qtz-Hbl fractionation and indicated equilibration temperature are typical of unaltered plutonic rocks (cf. Shieh 1985; Taylor 1987) and demonstrate $\delta^{18}O$ values for these minerals record subsolidus cooling with no discernible post-magmatic (i.e., hydrothermal) alteration. Values of Δ_{Qtz-Pl} and Δ_{Pl-Hbl} yield discordant temperatures (An_{60})

Table 6. Oxygen isotope data for Bristol Lake diorites

Sample	$\delta^{18}O_{V-SMOW}$ (per mil)
GR-036-WR	6.5
GR-036-Qtz[a]	9.4
GR-036-Pl[b]	6.6
GR-036-Hbl[c]	5.9
GR-035	7.0
GR-032	7.3
GR-022	7.1
GR-016	7.1
GR-006	7.6
GR-002	5.7
GR-009	7.0
BR-001	5.3
BR-002	5.8
NBR-001	4.7

[a] Qtz = quartz separate
[b] Pl = plagioclase separate
[c] Hbl = hornblende separate.

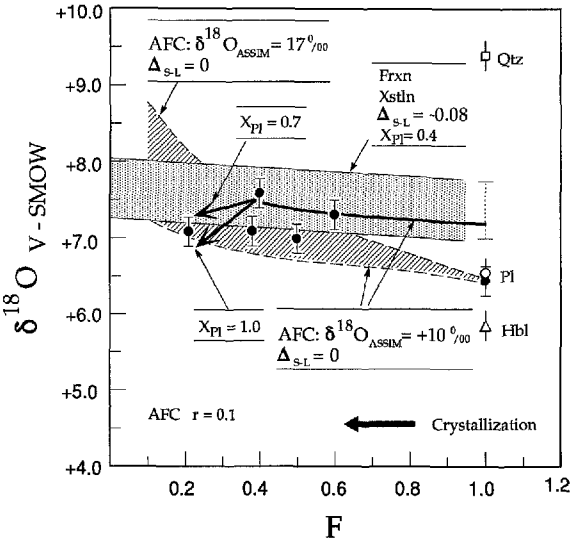

Fig. 13. Whole-rock and mineral separate $\delta^{18}O$ vs F for Granite Mountains diorites from Bull Canyon compared with calculated fractional crystallization and AFC evolutionary melt paths based on the fractionation factors of Muehlenbachs and Kushiro (1974) and model equations of DePaolo (1981) and Taylor and Sheppard (1986). The *dashed bracket* shows the whole-rock $\delta^{18}O$ of the most primitive diorite sample (GR-036) corrected for subsolidus alteration (see text). Solid-liquid fractionations (Δ_{S-L}) correspond to indicated weight fractions of Pl in the fractionating assemblage Pl + Hbl. *Black arrows* correspond to the two-stage AFC melt path depicted in Fig. 12 for an assimilate $\delta^{18}O$ of 10.0 per mil. *Stippled and hachured patterns* delimit ranges in fractional crystallization and AFC melt paths, respectively, emanating from possible initial melt compositions discussed in the text. Subscript, *Assim*, designates assimilate parameters

of 290 to 320°C (Matsuhisa et al. 1979) and ~ 800°C (Bottinga and Javoy 1975), respectively. Analytical uncertainties and uncertainties in equilibrium isotopic fractionation factors cannot account for the discrepancy. Plagioclase apparently has undergone ^{18}O depletion from an equilibrium $\delta^{18}O$ value of 7.4 to 7.9 per mil (based on equilibrium temperature recorded by $\Delta_{Qtz-Hbl}$ and fractionation calibrations cited above) to the measured value of 6.6 per mil. The occurrence of Pl with disequilibrium $\delta^{18}O$ coexisting with Qtz and Hbl which are in isotopic equilibrium with one another is characteristic of moderately hydrothermally altered plutonic rocks and reflects the greater rate of $^{18}O/^{16}O$ exchange between Pl and fluid relative to the other minerals (Gregory et al. 1989). Mass-balance constraints and modal abundances dictate that $\delta^{18}O^{WR}$ for this rock prior to feldspar alteration was 7.2 to 7.6 per mil, or 0.7 to 1.1 per mil higher than the present value (Fig. 13). The corrected $\delta^{18}O^{WR}$ for GR-036 is identical to the other diorites within analytical uncertainties. The range for the corrected value shown in Fig. 13 reflects the large uncertainties inherent in the calculation. Correction for subsolidus alteration in the primitive diorite sample demonstrates that variations in magmatic $\delta^{18}O$ are not resolvable in the Bull Canyon diorite suite.

Nominally magmatic and uniform $\delta^{18}O^{WR}$ in the Bull Canyon suite suggests that these rocks have not been *severely* affected by subsolidus $^{18}O/^{16}O$ exchange, but the fact that minor ^{18}O depletion occurred in one of the samples indicates that any magmatic trends in $\delta^{18}O$ that may have been present may well have been perturbed or erased.

The Granite Mountains diorite magmatic $\delta^{18}O$ values of 7.0 to 7.6 per mil are compatible with the AFC evolution derived from elemental and Sr isotopic data and are within 0.5 per mil of the parental magma value. These conclusions are demonstrated by evaluating the effects of both fractional crystallization and assimilation on the diorite melt $^{18}O/^{16}O$. For this purpose the fractionation factors between Pl and basaltic melt (L) and between enstatite (En) and L obtained by Muehlenbachs and Kushiro (1974) for magmatic temperatures of 1,000° can be used if it is assumed that $\Delta_{Hbl-L} \simeq \Delta_{En-L}$. The opposite signs and similar magnitudes of Δ_{En-L} and Δ_{Pl-L} combine to yield an effective solid-liquid $^{18}O/^{16}O$ fractionation (Δ_{S-L}) of ~ 0.0. The fractional crystallization melt paths for subequal Pl and Hbl therefore are consistent with the Granite Mountains coarse-grained diorite $\delta^{18}O^{WR}$ if the Pl-corrected whole-rock value for the primitive sample GR-036 is used (Fig. 13). The data are also consistent with the optimum AFC model if the assimilate $\delta^{18}O$ was no greater than 10 per mil and not significantly less than 7 per mil (Fig. 13). If the uncorrected $\delta^{18}O^{WR}$ for the primitive sample is used, an assimilate $\delta^{18}O$ of 10 to 17 per mil is permitted by the data (Fig. 13). Scatter in whole-rock $\delta^{18}O$ on the order of 0.5 per mil is expected for AFC melt paths produced by varied Pl/Hbl. For example, the two-stage AFC path involving an increase in Pl/Hbl suggested by the $(^{87}Sr/^{86}Sr)_i$ and Sr data (Fig. 12) produces a small shift from increasing to decreasing $\delta^{18}O$ with crystallization (black arrow, Fig. 13). As discussed above, it is unlikely that such small magmatic variations in $\delta^{18}O$ are discernible in these rocks.

In summary, the constant $\delta^{18}O$ (within uncertainties) of the Bull Canyon diorites prior to subsolidus alteration requires that any material assimilated during crystallization must have been similar to the diorite magma in $^{18}O/^{16}O$ or only moderately enriched in ^{18}O. The combined effects on magmatic $\delta^{18}O$ caused by fractional crystallization of Pl and Hbl and/or low rates of assimilation of moderately ^{18}O enriched material are ≤ 0.5 per mil (Fig. 13). The $\delta^{18}O$ for the diorite parental magma is therefore no lower than 6.5 and no greater than about 8.0 per mil with the most probable value being close to 7.2 per mil.

The assimilate

The essential features of the material assimilated by the Granite Mountains diorite magma are a high Sr concentration of 1,000 to 1,500 ppm, low Rb/Sr between 0.01 and 0.2, $^{87}Sr/^{86}Sr$ of about 0.7090 to 0.7200, and $\delta^{18}O$ of approximately 7 to 10 per mil. These characteristics constrain the origin of the assimilate but do not a priori correspond to assimilated rocks because of the potential for variable degrees of partial melting, multiple wall-rock minerologies, and variations in ambient *P-T*-fluid conditions (DePaolo 1981).

The moderate $\delta^{18}O$ of the assimilate precludes addition of mature metasedimentary rocks (Fig. 13). The assimilate also does not resemble the average crust of predominantly Proterozoic age (Farmer and DePaolo 1984) at the present-day level of exposure. Thirty samples representing a variety of Proterozoic rocks from the eastern Mojave Desert region (Wooden and Miller 1990; Wooden and Miller, unpublished) yield an average Sr concentration of 246 ppm, an average Rb/Sr of 0.42, and an average $^{87}Sr/^{86}Sr$ corrected to 155 Ma of 0.7293. None of these values are consistent with the model assimilate. In addition, a contaminant derived from partial melting would have an even higher Rb/Sr unless Pl ubiquitous in the presently exposed crust were entirely consumed.

The model assimilate does resemble present-day exposures of Mesozoic mafic lower crust in the southern Cordillera. Barth et al. (1991) described a sequence of mafic granulites representing lower crust from the San Gabriel Mountains of southern California. The mafic granulites are similar to the calculated assimilate in their high Sr, with an average of 614 ppm and ranging up to 1,044 ppm, average Rb/Sr of 0.04, and average Zr concentrations of 155 ppm. Concentrations of Ba, Nb, and Y are also comparable. Similarity between the mafic granulites and model assimilated material, especially in their high Sr and unusually low Rb/Sr, suggests that the best candidate for the assimilate is a mafic lower crustal granulite. The 7 to 10 per mil range of permissible $\delta^{18}O$ for the added material is consistent with assimilation of lower crustal granulites based on the data of Harmon and Fowler (1990) showing a mean $\delta^{18}O$ of 7.1 ± 0.8 per mil and a range of 5.9 to 8.6 per mil for lower crustal granulite xenoliths from Arizona.

The ca. 0.7090 minimum $^{87}Sr/^{86}Sr$ of the diorite assimilate is greater than the average Mesozoic San Gabriel granulite value of 0.7076 (Barth et al. 1991), suggesting the

presence of an older component in the assimilated mafic lower crust compared to the San Gabriel granulites. A younger average age for the San Gabriel complex is consistent with independent evidence indicating that some of its mafic plutonic protoliths post-date intrusion of the Bristol Lake diorites (Barth et al. 1991).

Samarium-neodymium isotopes

The Nd isotopic data for dioritic and associated granitic plutons in the Bristol Lake region analyzed in this study are summarized in Table 7. The initial ε_{Nd} values relative to chondrite uniform reservoir (CHUR) for the least evolved dioritic samples are among the least negative plutonic values obtained to date from the Mojave Desert region. These data bear upon the source of the diorites but are at present too few for inclusion in AFC models.

Source reservoirs

The isotopic data for the Granite Mountains diorites provide constraints on sources of the parental magma. Low $\delta^{18}O$ and the relatively positive ε_{Nd} point to a mantle or mafic lower-crustal source. Possible end-member isotopic reservoirs which may have contributed to the parental magma by partial melting or assimilation include suboceanic mantle reservoirs (including asthenosphere and subducted MORB), subcontinental lithospheric mantle, and lower and middle to upper crust of dominantly Proterozoic age. Fields delimiting the radiogenic isotopic character of these reservoirs corrected to an age of 155 Ma are shown in Fig. 14. Uncertainties in age on the order 100 Ma do not affect significantly positions of plotted values of $\varepsilon_{Nd}(t)$ or $(^{87}Sr/^{86}Sr)_t$ in Fig. 14.

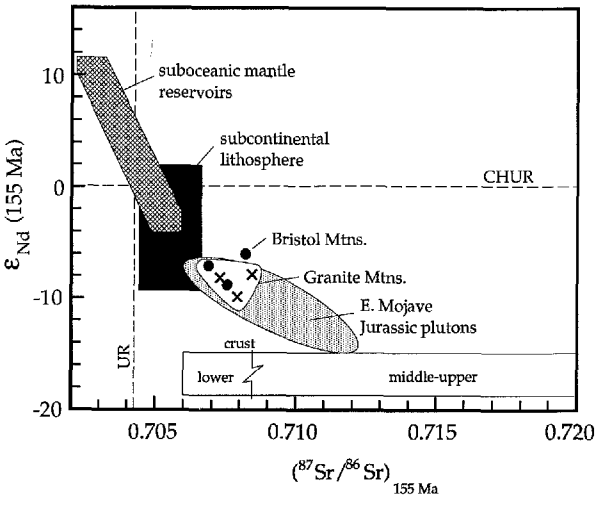

Fig. 14. Time-corrected $\varepsilon_{Nd}(t)$ and $^{87}Sr/^{86}Sr_i$ isotopic reservoirs for diorite plutons in the Bristol Lake region. Derivations of fields are presented in the text. The initial isotopic compositions of Jurassic diorites from the Granite and Bristol Mountains (●), associated Late Jurassic-earliest Early Cretaceous sphene granite and porphyritic monzogranite from the Granite Mountains (Young 1990, ×), and the field for eastern Mojave Desert Jurassic plutons (Wooden, unpublished) are shown for comparison

Suboceanic mantle sources in Fig. 14 are represented by modern oceanic basalts [MORB (mid-ocean-ridge basalt), OIB (ocean-island basalt), White and Hoffman 1982]. The field for subcontinental lithosphere is defined by the Cenozoic continental alkali basalts of the Sierra Nevada Province described by Menzies et al. (1983). Menzies et al.; Musselwhite et al. (1989), and Farmer et al. (1989) have argued that these lavas were emplaced during incipient rifting of the southern Cordilleran continental crust, and are therefore likely to represent melts derived from a subcontinental lithosphere isolated since the early Middle Proterozoic. The localities from which these data were obtained lie within the region yielding Sm-Nd model ages of 2.0 to 2.3 Ga defined by Bennett and DePaolo (1985), as does the Bristol Lake region (cf. Musselwhite et al. 1989). The inferred subcontinental material is characterized by low Sm/Nd and high Rb/Sr relative to CHUR and the Sr-isotopic uniform mantle reservoir (UR) defined by DePaolo and Wasserburg (1976) (Fig. 14), and may be a sub-Moho "lower crust" or mantle keel (e.g., DePaolo 1981) with geochemical properties distinct from typical mantle. The Sr isotope data of Menzies et al. (1983) have been corrected to an age of 155 Ma using Rb/Sr = 0.036 based on typical enriched peridotites (e.g. Brophy and Marsh 1986). The corresponding Nd isotope data have not been corrected for age because of the uncertainty in the precise extent of LREE enrichment but such corrections would be small. A change in ε_{Nd} of -0.1 in 155 Ma corresponds to an enrichment factor $f_{Sm/Nd}$ (defined by DePaolo and Wasserburg 1976; see Table 7) relative to CHUR of -0.026. The continental crust isotopic reservoir was defined using data for Proterozoic rocks in the eastern Mojave Desert region (Bennett and DePaolo 1987; Davis et al. 1982; Wooden and Miller, unpublished). The lower-crustal subfield in Fig. 14 is based on the premise that this portion of the crust was depleted in Rb during high-grade metamorphism (DePaolo 1981; Barth et al. 1991).

The position of the diorite samples relative to the reservoirs defined above in $\varepsilon_{Nd}(t)$ – $(^{87}Sr/^{86}Sr)_i$ space suggests several possibilities for their source (Fig. 14). The simplest interpretation is that the diorite parental magma was derived from subcontinental lithosphere enriched in LREE and Rb. The diorites lie just outside the margin of this field with respect to radiogenic Sr, possibly reflecting assimilation of small amounts of ancient crustal material as suggested by AFC modeling of the suite. Kyser et al. (1982) cite evidence that subcontinental lithosphere is characterized by $\delta^{18}O$ higher than typical MORB values of 5.7 ± 0.3 per mil and is probably near 7.0 per mil. Unaltered diorite $\delta^{18}O$ values of about 7.2 per mil are consistent with this lower continental lithosphere value in view of the small degree of oxygen isotope fractionation expected during partial melting (Taylor and Sheppard 1986). The low Hf/Ba and Zr/Ba ratios of the basaltic diorites are also consistent with the inferred source in that these attributes were considered by Farmer et al. (1989) and Ormerod et al. (1988) to be diagnostic of basalts derived from subcontinental lithosphere.

Table 7. Nd isotope data for Bristol Lake diorites and granites

Sample	Sm ppm	Nd ppm	$^{147}Sm/^{144}Nd$	$^{143}Nd/^{144}Nd$	ε_{meas}[a]	$f_{Sm/Nd}$[b]	age (Ma)	ε_i[c]
GR-036	4.93	21.64	0.1382	0.512211	− 8.4	− 0.2974	155	− 7.2
GR-006	7.04	38.05	0.1180	0.512141	− 9.7	− 0.4001	155	− 8.1
GR-004	8.28	42.64	0.1174	0.512103	− 10.4	− 0.4032	155	− 8.8
BR-001	6.27	29.24	0.1296	0.512257	− 7.4	− 0.3411	155	− 6.1
GR-018[d]	8.17	49.11	0.1206	0.512157	− 9.4	− 0.3869	142	− 8.0
GR-030[d]	7.59	43.78	0.1048	0.512118	− 10.1	− 0.4672	142	− 8.4
GR-023[d]	11.69	62.47	0.1131	0.512054	− 11.4	− 0.4250	142	− 9.9

[a] ε is the deviation in parts per 10^4 from the CHUR mantle reservoir where $(^{143}Nd/^{144}Nd)_{CHUR}(t)$ is calculated from present-day $(^{143}Nd/^{144}Nd)^0_{CHUR} = 0.512638$ and $(^{147}Sm/^{144}Nd)^0_{CHUR} = 0.1967$

[b] Fractionation factor $f_{Sm/Nd}$ defined as $(^{147}Sm/^{144}Nd)_{sample}/^{147}Sm/^{144}Nd)_{CHUR} - 1$

[c] Initial value based on $\lambda_{Sm} = 6.54 \times 10^{-12}$ year^{-1}

[d] Granitic plutons from the Granite Mountains shown in Fig. 1

Descriptions of plutons given by Young (1990)

The Sr and Nd isotopic data for Late Jurassic granite and monzogranite plutons analyzed from the Bristol Lake region are similar to the diorites (Fig. 14). Isotopic data for 210 Ma to 150 Ma dioritic and granitic plutons from the Mojave Desert of southeastern California as a whole (Wooden unpublished) define an array between the fields for subcontinental lithosphere and continental crust in Fig. 14. The array suggests that mixing between these isotopic reservoirs may have been an important process during Jurassic pluton formation in the region. Generation of magmas in the subcontinental lithosphere implies extension of the crust (Lum et al. 1989; McDonough 1990) and is consistent with the proposal by Busby-Spera (1988) that the eastern Mojave Desert was a zone of protracted intra-arc extension during this time period.

Source lithology

The low Mg number {molecular 100[Mg/(Mg + Fe)]} of 51 for the least fractionated members of the diorite suite preclude equilibration with a mantle source containing olivine or orthopyroxene (e.g. Frey et al. 1978). Vaniman et al. (1982) showed that fractionation of amphibole can explain low Mg numbers and low Ti concentrations of evolved hawaiite magmas compositionally similar to the Bristol Lake diorites relative to their parental magmas. The prominent role of Hbl in the evolution of the diorites therefore suggests that the primitive compositions identified in this study are themselves derivatives of an unseen parent. Since the true parental melt apparently is not exposed, the major residual phases of its source can be only loosely constrained.

The high water contents indicated by early crystallization of hornblende suggest that the source was hydrous. The LREE- and Rb-enriched lithosphere was thus apparently metasomatized. Schulze (1989) found that the bulk abundance of eclogite in subcontinental lithosphere is probably small (i.e., < 1% by volume). For these reasons, the favored lithology for the source rock of the diorite parental magmas of the Bristol Lake region is a hydrous LREE-enriched peridotite. Van Kooten (1981), Vaniman et al. (1982), and Menzies et al. (1983) discussed the evidence for a hydrous mica or amphibole-bearing garnet-clinopyroxene source for the lavas used to model the isotopic composition of the subcontinental lithosphere in the eastern Mojave Desert.

The incompatible behavior of Zr (Table 3) allows the Zr concentration of the primitive diorite samples to be used as maximum concentrations for the actual parental melt. With this in mind the data suggest that Zrn was not a residual phase following partial melting of the subcontinental lithospheric source. For example, a reasonable near-liquidus temperature of 1,000°C (e.g., Russell and Nicholls 1985) would require a melt Zr concentration of 507 ppm for Zrn saturation compared with only 81 ppm for the primitive sample GR-036 (Watson and Harrison 1983, 1984). Undersaturation in Zr could have resulted in resorption of entrained zircons during the assimilation process and is consistent with the paucity of inherited Zrn evidenced in the U-Pb isotope systematics.

Conclusions

Late Jurassic dioritic rocks from the Bristol Lake region share several geochemical attributes with high-alumina basalts, high-K arc andesites, and continental hawaiite basalts. The 155 Ma diorite pluton from the Granite Mountains evolved by combined assimilation and fractional crystallization of hornblende and plagioclase. A Monte Carlo method for obtaining optimum inverse solutions to the AFC model equations of DePaolo (1981) indicates that the assimilate resembled ancient lower crustal mafic granulites and that the mass ratio of assimilated crust to parental magma was on the order of 0.1. Lack of enrichment in $\delta^{18}O$ during differentiation is consistent with these model calculations.

Oxygen, Sr, and Nd isotopic data and trace-element concentrations point to a subcontinental lithospheric source for the Granite Mountains diorite parental magma. The source was composed of metasomatized hydrous peridotite enriched in light-rare-earth elements and Rb. Diorites from neighboring ranges may have been derived from similar sources. Comparison with Sr and Nd isotopic compositions of other plutons from the eastern

Mojave Desert suggests that continental lithosphere may have been an important component of Jurassic pluton generation in the region. Emplacement of magmas derived from the subcontinental lithosphere into the crust is consistent with suggestions that the eastern Mojave Desert was part of a zone of protracted intra-arc extension during the Jurassic.

Acknowledgements. This paper is the product of a portion of the first author's Ph.D. dissertation conducted at the University of Southern California under the direction of J. Lawford Anderson. Financial support was provided by NSF grant EAR 86-18285 to Professor J. L. Anderson, grants from the Geological Society of America and Sigma Xi, and the University of Southern California Research Fund. S. Katz provided help with the Monte Carlo optimization modeling. We wish to thank J. L. Anderson, R. M. Tosdal, K. A. Howard, A. P. Barth, and M. Davidson for helpful discussions throughout this study. Thoughful critiques by C. F. Miller and an anonymous reviewer are greatly appreciated and resulted in significant improvement over the original manuscript.

References

Barca D, Crisci GM, Ranieri GA (1988) Further developments of the Rayleigh equation for fractional crystallization. Earth Planet Sci Lett 89:170–172

Barth AP, Wooden JL, May DJ (1992) Small scale heterogeneity of Phanerozoic lower crust: evidence from isotopic and geochemical systematics of mid-Cretaceous granulite gneisses, San Gabriel Mountains, southern California, Contrib Mineral Petrol (in press)

Bennett VC, DePaolo DJ (1986) Implications of Nd isotopes for the crustal history of southern California (abstract). Geol Soc Am Abstr 18:84

Bennett VC DePaolo DJ (1987) Proterozoic crustal history of the western United States as determined by neodymium isotopic mapping. Geol Soc Am Bull 99:674–685

Bhattacharyya GK, Johnson RA (1977) Statistical concepts and methods. Wiley & Sons, New York: 639

Bottinga Y, Javoy M (1975) Oxygen isotope partitioning among the minerals in igneous and metamorphic rocks. Rev Geophys Space Phys 13:401–418

Brophy JG, Marsh BD (1986) On the origin of high alumina arc basalt and the mechanics of melt extraction. J Petrol 27:763–790

Busby-Spera CJ (1988) Speculative tectonic model for the early Mesozoic arc of the south-west Cordilleran United States. Geology 16:1121–1125

Chayes F (1971) Ratio correlation: a manual for students of petrology and geochemistry. University of Chicago Press, Chicago

Clayton RN, Mayeda TK (1963) The use of bromine pentafluoride in the extraction of oxygen from oxides and silicates for isotope analysis. Geochim Cosmochim Acta 27:43–52

Cocherie A (1986) Systematic use of trace element distribution patterns in log-log diagrams for plutonic suites. Geochim Cosmochim Acta 50:2517–2522

Collins WJ, Beams SD, White AJR, Chappell BW (1982) Nature and origin of A-type granites with particular reference to southeastern Australia. Contrib Mineral Petrol 80:189–200

Davis GA, Anderson JL, Krummenacher D, Frost EG, Armstrong RL (1982) Geologic and geochronologic relations in the lower plate of the Whipple detachment fault, Whipple Mountains, southeastern California, a progress report. In: Frost EG, Martin DL (eds) Mesozoic–Cenozoid tectonic evolution of the Colorado River region, California, Arizona, and Nevada. Cordilleran Publishers, San Diego, 408–432

DePaolo DJ (1981) Trace element and isotopic effects of combined wallrock assimilation and fractional crystallization. Earth Planet Sci Lett 53:189–202

DePaolo DJ, Wasserburg GJ (1976) Nd isotopic variations and petrogenetic models. Geo-phys Res Lett 3:249–252

Ernst RE, Fowler AD, Pearce TH (1988) Modelling of igneous fractionation and other processes using Pearce diagrams. Contrib Mineral Petrol 100:12–18

Farmer GL, DePaolo DJ (1983) Origin of Mesozoic and Tertiary granite in the western United States and implications for pre-Mesozoic crustal structure 1: Nd and Sr isotopic studies in the geocline of the northern Great Basin. J Geophys Res 88:3379–3401

Farmer GL, DePaolo DJ (1984) Origin of Mesozoic and Tertiary granite in the western US and implications for pre-Mesozoic crustal structure 2: Nd and Sr isotopic studies of unmineralized and Cu- and Mo-mineralized granite in the Precambrian craton. J. Geophys Res 89:10141–10160

Farmer GL, Perry FV, Semken S, Crowe B, Curtis D, DePaolo DJ (1989) Isotopic evidence on the structure and origin of subcontinental lithospheric mantle in southern Nevada. J Geophys Res 94:7885–7898

Fox LK, Miller DM (1990) Jurassic granitoids and related rocks of the southern Bristol Mountains, southern Providence Mountains, and Colton Hills, Mojave Desert, California. In: Anderson JL (ed) The nature and origin of cordilleran magmatism. Geol Soc Am Mem 174:111–132

Frey FA, Green DH, Roy S (1978) Integrated models of basalt petrogenesis: a study of quartz tholeiites to olivine melilites from southeastern Australia utilizing geochemical and experimental petrologic data. J Petrol 19:463–513

Gill JB (1981) Orogenic andesites and plate tectonics. Springer-Verlag, New York

Gregory RT, Criss RE, Taylor HP (1989) Oxygen isotope exchange kinetics of mineral pairs in closed and open systems: applications to problems of hydrothermal alteration of igneous rocks and Precambrian iron formations. Chem Geol 75:1–42

Harmon RS, Fowler MB (1990) Oxygen isotope composition of the lower crust (abstract) Gold-schmidt Conf 2 Abstr:51

Harvey PK, Taylor DM, Hendry RD, Bancroft F (1973) An accurate fusion method for the analysis of rocks and chemically related materials by X-ray fluorescence spectrometry. X-ray Spectrom 2:33–34

Heinrich KFJ (1964) Expanded preprint to WR Van Schmus of tables of mass absorption coefficients for K-alpha lines by Heinrich KFJ, Vieth DL, Yakowitz H. In: Mallet GR, Fay MJ, Mueller WM (eds) Advances in X-ray analysis. Plenum, New York

Henderson P (1982) Inorganic geochemistry. Pergamon, Oxford

Howard KA, Kilburn JE, Simpson RW, Fitzgibbon TT, Detra DE, Raines GL, Sabine C (1989) Mineral resources of part of the Bristol/Granite Mountains wilderness study area, San Bernardino County, California. US Geol Sur Bull 1712-C

John GE (1981) Reconnaissance study of Mesozoic plutonic rocks in the Mojave Desert region. In: Howard KA et al (eds) Tectonic framework of the Mojave and Sonoran deserts, California and Arizona. US Geol Surv Open-File Rep 81–503:49–51

Kay SM, Kay RW, Citron GP (1982) Tectonic controls on tholeiitic and calc-alkaline magmatism in the Aleutian Arc. J Geophys Res 87:4051–4072

Kretz R (1983) Symbols for rock-forming minerals. Am Mineral 68:277–279

Krogh TE (1973) A low contamination method for the hydrothermal decomposition of zircon and extraction of U and Pb for isotopic age determinations. Geochim Cosmochim Acta 37:485–494

Kyser TK, O'Neil JR, Carmichael ISE (1982) Genetic relations among basic lavas and ultramafic nodules: evidence from oxygen isotope compositions. Contrib Mineral Petrol 81:88–102

Langmuir CH, Vocke RD Jr, Hanson GN (1978) A general mixing equation with applications to Icelandic basalts. Earth Planet Sci Lett 37:380–392

Le Maitre RW (1982) Numerical petrology, statistical interpretation of geochemical data. (Developments in petrology 8) Elsevier, New York

Ludwig KR (1980) Calculation of uncertainties of U-Pb isotope data. Earth Planet Sci Lett 46:212–220
Lum CCL, Leeman WP, Foland KA, Kargel JA, Fitton JG (1989) Isotopic variations in continental basaltic lavas as indicators of mantle heterogeneity: examples from the western U.S. Cordillera. J Geophys Res 94:7871–7884
Marquardt DW (1963) An algorithm for least squares estimation of non-linear parameters. J Soc Ind Appl Math 11:431–441
Matsuhisa Y, Goldsmith JR, Clayton RN (1979) Oxygen isotope fractionation in the system quartz-albite-anorthite-water. Geochim Cosmochim Acta 43:1131–1140
McDonough WF (1990) Constraints on the composition of the continental lithospheric mantle. Earth Planet Sci Lett 101:1–18
Menzies MA, Leeman WP, Hawkesworth CJ (1963) Isotope geochemistry of Cenozoid volcanic rocks reveals mantle heterogeneity below western USA. Nature 303:205–209
Meschede M (1986) A method of discriminating between different types of mid-ocean ridge basalts and continental tholeiites with the Nb-Zr-Y diagram. Chem Geol 56:207–218
Miller DM, Glick LL, Goldfarb R, Simpson RW, Hoover DB, Detra DE, Dohrenwend JC, Munts SR (1985) Mineral resources and resource potential map of the south Providence Mountains wilderness study area, San Bernardino County, California. Misc Field Studies Map US Geol Surv MF-1780-A:
Miller CF, Wooden JL, Bennett VC, Wright JE, Solomon GC, Hurst RW (1990) Petrogenesis of the composite peraluminous-metaluminous Old Woman-Piute Range batholith, southeastern California; isotopic constraints. In Anderson JL (ed) The nature and origin of Cordilleran magmatism. Geol Soc Am Mem 174:99–109
Minster JF, Minster JB, Treuil M, Allegre CJ (1977) Systematic use of trace elements in igneous processes. Contrib Mineral Petrol 61:49–77
Muehlenbachs K, Kushiro I (1974) Oxygen isotope exchange and equilibrium of silicates with CO_2 and O_2. Carnegie Inst Washington Yearb 72:232–236
Musselwhite DS, DePaolo DJ, McCurry M (1989) The evolution of a silicic magma system: isotopic and chemical evidence from the Woods Mountains volcanic center, eastern California. Contrib Mineral Petrol 101:19–29
Nicholls IA, Harris KL (1980) Experimental rare earth element partition coefficients for garnet, clinopyroxene and amphibole coexisting with andesitic and basaltic liquids. Geochim Cosmochim Acta 44:287–308
Nicholls J (1988) The statistics of Pearce element diagrams and the Chayes closure problem. Contrib Mineral Petrol 99:11–24
Norrish K, Hutton JT (1969) An accurate X-ray spectrographic method for the analysis of a wide range of geological samples. Geochim Cosmochim Acta 33:431–453
Ormerod DS, Hawkesworth CJ, Rogers NW, Leeman WP, and Menzies MA (1988) Tectonic and magmatic transitions in the western Great Basin, USA. Nature 333:349–353
Pearce JA, Norry MJ (1979) Petrogenetic implications of Ti, Zr, Y, and Nb variations in volcanic rocks. Contrib Mineral Petrol 69:33–47
Pharaoh TC, Pearce JA (1984) Geochemical evidence for the geotectonic setting of early Proterozoic metavolcanic sequences in Lapland. Precambrian Res 25:283–308
Press F (1968) Earth models obtained by Monte Carlo inversion. J Geophys Res 73:5223–5234
Russell JK, Nicholls J (1985) Application of Duhem's theorem to the estimation of extensive and intensive properties of basaltic magmas. Can Mineral 23:479–488
Russell JK, Nicholls J (1988) Analysis of petrologic hypotheses with Pearce element ratios. Contrib Mineral Petrol 99:25–35
Schulze DJ (1989) Constraints on the abundance of ecologite in the upper mantle. J Geophys Res 94:4205–4213
Shieh Y-N (1985) High-^{18}O granitic plutons from the Frontenac Axis, Grenville Province of Ontario, Canada, Geochim Cosmochim Acta 49:117–123
Streckeisen AL (1976) To each plutonic rock its proper name. Earth-Sci Rev 12:1–33
Taylor HP Jr (1987) Comparison of hydrothermal systems in layered gabbros and granites, and the origin of low ^{18}O magmas. In: Mysen BO (ed) Magmatic processes: physicochemical principles. Geochem Soc Special Pub No 1. Lancaster Press: 337–357
Taylor HP, Sheppard SMF (1986) Igneous rocks; I: processes of isotopic fractionation and isotope systematics. In: Valley JW, Taylor HP, O'Neil JR (eds) Stable isotope in high temperature geological processes (Reviews in Mineralogy 16) Mineral Soc Am, Washington, D.C., pp 227–271
Vaniman DT, Crowe BM, Gladney ES (1982) Petrology and geochemistry of hawaiite lavas from Crater Flat, Nevada. Contrib Mineral Petrol 80:341–357
Van Kooten GK (1981) Pb and Sr systematics of ultrapotassic and basaltic rocks from the central Sierra Nevada, California. Contrib Mineral Petrol 76:378–385
Watson EB, Harrison TM (1983) Zircon saturation revisited: temperature and composition effects in a variety of crustal magma types. Earth Planet Sci Lett 64:295–304
Watson EB, Harrison TM (1984) Accessory minerals and the geochemical evolution of crustal magmatic systems: a summary and prospects of experimental approaches. Phys Earth Planet Inter 35:19–30
White WM, Hoffman AW (1982) Sr and Nd isotope geochemistry of oceanic basalts and mantle evolution. Nature 296:821–825
Wooden JL, Miller DM (1990) Chronologic and isotopic framework for Early Proterozoic crustal evolution in the eastern Mojave Desert region, SE California. J Geophys Res 95:20133–20146
Wyers GP, Barton M (1989) Polybaric evolution of calc-alkaline magmas from Nisyros, southeastern Hellenic arc, Greece. J Petrol 30:1–38
Young ED (1990) Geothermobarometric and geochemical studies of two crystalline terrains of the eastern Mojave Desert, USA. Unpubl PhD dissertation, Univ of Southern California, Los Angeles

Editorial responsibility: J. Ferry